Karolchik, D., Bruen, T. C., Bevan, R., Cutler, D. J., Schwartz, S., Elnitski, L., Idol, J. R., Prasad, A. B., Lee-Lin, S. Q., Maduro, V. V., Summers, T. J., Portnoy, M. E., Dietrich, N. L., Akhter, N., Ayele, K., Benjamin, B., Cariaga, K., Brinkley, C. P., Brooks, S. Y., Granite, S., Guan, X., Gupta, J., Haghighi, P., Ho, S. L., Huang, M. C., Karlins, E., Laric, P. L., Legaspi, R., Lim, M. J., Maduro, Q. L., Masiello, C. A., Mastrian, S. D., McCloskey, J. C., Pearson, R., Stantripop, S., Tiongson, E. E., Tran, J. T., Tsurgeon, C., Vogt, J. L., Walker, M. A., Wetherby, K. D., Wiggins, L. S., Young, A. C., Zhang, L. H., Osoegawa, K., Zhu, B., Zhao, B., Shu, C. L., De Jong, P. J., Lawrence, C. E., Smit, A. F., Chakravarti, A., Haussler, D., Green, P., Miller, W., and Green, E. D. (2003) Comparative analyses of multi-species sequences from targeted genomic regions. *Nature* **424,** 788–793

27. Woolfe, A., Goodson, M., Goode, D. K., Snell, P., McEwen, G. K., Vavouri, T., Smith, S. F., North, P., Callaway, H., Kelly, K., Walter, K., Abnizova, I., Gilks, W., Edwards, Y. J., Cooke, J. E., and Elgar, G. (2005) Highly conserved non-coding sequences are associated with vertebrate development. *PLoS Biol.* **3,** e7
28. Bell, A. C., West, A. G., and Felsenfeld, G. (1999) The protein CTCF is required for the enhancer blocking activity of vertebrate insulators. *Cell* **98,** 387–396
29. Felsenfeld, G., Burgess-Beusse, B., Farrell, C., Gaszner, M., Ghirlando, R., Huang, S., Jin, C., Litt, M., Magdinier, F., Mutskov, V., Nakatani, Y., Tagami, H., West, A., and Yusufzai, T. (2004) Chromatin boundaries and chromatin domains. *Cold Spring Harb. Symp. Quant. Biol.* **69,** 245–250
30. Shen, Y., Yue, F., McCleary, D. F., Ye, Z., Edsall, L., Kuan, S., Wagner, U., Dixon, J., Lee, L., Lobanenkov, V. V., and Ren, B. (2012) A map of the cis-regulatory sequences in the mouse genome. *Nature* **488,** 116–120
31. Birney, E., Stamatoyannopoulos, J. A., Dutta, A., Guigo, R., Gingeras, T. R., Margulies, E. H., Weng, Z., Snyder, M., Dermitzakis, E. T., Thurman, R. E., Kuehn, M. S., Taylor, C. M., Neph, S., Koch, C. M., Asthana, S., Malhotra, A., Adzhubei, I., Greenbaum, J. A., Andrews, R. M., Flicek, P., Boyle, P. J., Cao, H., Carter, N. P., Clelland, G. K., Davis, S., Day, N., Dhami, P., Dillon, S. C., Dorschner, M. O., Fiegler, H., Giresi, P. G., Goldy, J., Hawrylycz, M., Haydock, A., Humbert, R., James, K. D., Johnson, B. E., Johnson, E. M., Frum, T. T., Rosenzweig, E. R., Karnani, N., Lee, K., Lefebvre, G. C., Navas, P. A., Neri, F., Parker, S. C., Sabo, P. J., Sandstrom, R., Shafer, A., Vetrie, D., Weaver, M., Wilcox, S., Yu, M., Collins, F. S., Dekker, J., Lieb, J. D., Tullius, T. D., Crawford, G. E., Sunyaev, S., Noble, W. S., Dunham, I., Denoeud, F., Reymond, A., Kapranov, P., Rozowsky, J., Zheng, D., Castelo, R., Frankish, A., Harrow, J., Ghosh, S., Sandelin, A., Hofacker, I. L., Baertsch, R., Keefe, D., Dike, S., Cheng, J., Hirsch, H. A., Sekinger, E. A., Lagarde, J., Abril, J. F., Shahab, A., Flamm, C., Fried, C., Hackermuller, J., Hertel, J., Lindemeyer, M., Missal, K., Tanzer, A., Washietl, S., Korbel, J., Emanuelsson, O., Pedersen, J. S., Holroyd, N., Taylor, R., Swarbreck, D., Matthews, N., Dickson, M. C., Thomas, D. J., Weirauch, M. T., Gilbert, J., Drenkow, J., Bell, I., Zhao, X., Srinivasan, K. G., Sung, W. K., Ooi, H. S., Chiu, K. P., Foissac, S., Alioto, T., Brent, M., Pachter, L., Tress, M. L., Valencia, A., Choo, S. W., Choo, C. Y., Ucla, C., Manzano, C., Wyss, C., Cheung, E., Clark, T. G., Brown, J. B., Ganesh, M., Patel, S., Tammana, H., Chrast, J., Henrichsen, C. N., Kai, C., Kawai, J., Nagalakshmi, U., Wu, J., Lian, Z., Lian, J., Newburger, P., Zhang, X., Bickel, P., Mattick, J. S., Carninci, P., Hayashizaki, Y., Weissman, S., Hubbard, T., Myers, R. M., Rogers, J., Stadler, P. F., Lowe, T. M., Wei, C. L., Ruan, Y., Struhl, K., Gerstein, M., Antonarakis, S. E., Fu, Y., Green, E. D., Karaoz, U., Siepel, A., Taylor, J., Liefer, L. A., Wetterstrand, K. A., Good, P. J., Feingold, E. A., Guyer, M. S., Cooper, G. M., Asimenos, G., Dewey, C. N., Hou, M., Nikolaev, S., Montoya-Burgos, J. I., Loytynoja, A., Whelan, S., Pardi, F., Massingham, T., Huang, H., Zhang, N. R., Holmes, I., Mullikin, J. C., Ureta-Vidal, A., Paten, B., Seringhaus, M., Church, D., Rosenbloom, K., Kent, W. J., Stone, E. A., Batzoglou, S., Goldman, N., Hardison, R. C., Haussler, D., Miller, W., Sidow, A., Trinklein, N. D., Zhang, Z. D., Barrera, L., Stuart, R., King, D. C., Ameur, A., Enroth, S., Bieda, M. C., Kim, J., Bhinge, A. A., Jiang, N., Liu, J., Yao, F., Vega, V. B., Lee, C. W., Ng, P., Shahab, A., Yang, A., Moqtaderi, Z., Zhu, Z., Xu, X., Squazzo, S., Oberley, M. J., Inman, D., Singer, M. A., Richmond, T. A., Munn, K. J., Rada-Iglesias, A., Wallerman, O., Komorowski, J., Fowler, J. C., Couttet, P., Bruce, A. W., Dovey, O. M., Ellis, P. D., Langford, C. F., Nix, D. A., Euskirchen, G., Hartman, S., Urban, A. E., Kraus, P., Van Calcar, S., Heintzman, N., Kim, T. H., Wang, K., Qu, C., Hon, G., Luna, R., Glass, C. K., Rosenfeld, M. G., Aldred, S. F., Cooper, S. J., Halees, A., Lin, J. M., Shulha, H. P., Zhang, X., Xu, M., Haidar, J. N., Yu, Y., Ruan, Y., Iyer, V. R., Green, R. D., Wadelius, C., Farnham, P. J., Ren, B., Harte, R. A., Hinrichs, A. S., Trumbower, H., Clawson, H., Hillman-Jackson, J., Zweig, A. S., Smith, K., Thakkapallayil, A., Barber, G., Kuhn, R. M., Karolchik, D., Armengol, L., Bird, C. P., de Bakker, P. I., Kern, A. D., Lopez-Bigas, N., Martin, J. D., Stranger, B. E., Woodroffe, A., Davydov, E., Dimas, A., Eyras, E., Hallgrimsdottir, I. B., Huppert, J., Zody, M. C., Abecasis, G. R., Estivill, X., Bouffard, G. G., Guan, X., Hansen, N. F., Idol, J. R., Maduro, V. V., Maskeri, B., McDowell, J. C., Park, M., Thomas, P. J., Young, A. C., Blakesley, R. W., Muzny, D. M., Sodergren, E., Wheeler, D. A., Worley, K. C., Jiang, H., Weinstock, G. M., Gibbs, R. A., Graves, T., Fulton, R., Mardis, E. R., Wilson, R. K., Clamp, M., Cuff, J., Gnerre, S., Jaffe, D. B., Chang, J. L., Lindblad-Toh, K., Lander, E. S., Koriabine, M., Nefedov, M., Osoegawa, K., Yoshinaga, Y., Zhu, B., and de Jong, P. J. (2007) Identification and analysis of functional elements in 1% of the human genome by the ENCODE pilot project. *Nature* **447,** 799–816
32. Blow, M. J., McCulley, D. J., Li, Z., Zhang, T., Akiyama, J. A., Holt, A., Plajzer-Frick, I., Shoukry, M., Wright, C., Chen, F., Afzal, V., Bristow, J., Ren, B., Black, B. L., Rubin, E. M., Visel, A., and Pennacchio, L. A. (2010) ChIP-Seq identification of weakly conserved heart enhancers. *Nat. Genet.* **42,** 806–810
33. Koch, F., Jourquin, F., Ferrier, P., and Andrau, J. C. (2008) Genome-wide RNA polymerase II: not genes only!. *Trends Biochem. Sci.* **33,** 265–273
34. Szutorisz, H., Dillon, N., and Tora, L. (2005) The role of enhancers as centres for general transcription factor recruitment. *Trends Biochem. Sci.* **30,** 593–599
35. Sei, C. A., Irons, C. E., Sprenkle, A. B., McDonough, P. M., Brown, J. H., and Glembotski, C. C. (1991) The α-adrenergic stimulation of atrial natriuretic factor expression in cardiac myocytes requires calcium influx, protein kinase C, and calmodulin-regulated pathways. *J. Biol. Chem.* **266,** 15910–15916
36. Iaccarino, G., Dolber, P. C., Lefkowitz, R. J., and Koch, W. J. (1999) Bβ-adrenergic receptor kinase-1 levels in catecholamine-induced myocardial hypertrophy: regulation by beta- but not alpha1-adrenergic stimulation. *Hypertension* **33,** 396–401
37. Seidman, C. E., Wong, D. W., Jarcho, J. A., Bloch, K. D., and Seidman, J. G. (1988) *Cis*-acting sequences that modulate atrial natriuretic factor gene expression. *Proc. Natl. Acad. Sci. U. S. A.* **85,** 4104–4108
38. Thuerauf, D. J., and Glembotski, C. C. (1997) Differential effects of protein kinase C, Ras, and Raf-1 kinase on the induction of the cardiac B-type natriuretic peptide gene through a critical promoter-proximal M-CAT element. *J. Biol. Chem.* **272,** 7464–7472

Received for publication November 12, 2013.
Accepted for publication January 2, 2014.

Evaluation of intramitochondrial ATP levels identifies G0/G1 switch gene 2 as a positive regulator of oxidative phosphorylation

Hidetaka Kioka[a,b,1], Hisakazu Kato[a,1], Makoto Fujikawa[c], Osamu Tsukamoto[a], Toshiharu Suzuki[d,e], Hiromi Imamura[f], Atsushi Nakano[a,g], Shuichiro Higo[a,b], Satoru Yamazaki[h], Takashi Matsuzaki[b], Kazuaki Takafuji[i], Hiroshi Asanuma[j], Masanori Asakura[g], Tetsuo Minamino[b], Yasunori Shintani[a], Masasuke Yoshida[e], Hiroyuki Noji[k], Masafumi Kitakaze[g], Issei Komuro[b,l], Yoshihiro Asano[a,b,2], and Seiji Takashima[a,2]

Departments of [a]Medical Biochemistry and [b]Cardiovascular Medicine and [i]Center for Research Education, Osaka University Graduate School of Medicine, Osaka 565-0871, Japan; [c]Department of Biochemistry, Faculty of Pharmaceutical Science, Tokyo University of Science, Chiba 278-8510, Japan; [d]Chemical Resources Laboratory, Tokyo Institute of Technology, Yokohama 226-8503, Japan; [e]Department of Molecular Bioscience, Kyoto Sangyo University, Kyoto 603-8555, Japan; [f]The Hakubi Center for Advanced Research and Graduate School of Biostudies, Kyoto University, Kyoto 606-8501, Japan; Departments of [g]Clinical Research and Development and [h]Cell Biology, National Cerebral and Cardiovascular Center Research Institute, Osaka 565-8565, Japan; [j]Department of Cardiovascular Science and Technology, Kyoto Prefectural University School of Medicine, Kyoto 602-8566, Japan; and [k]Department of Applied Chemistry, School of Engineering and [l]Department of Cardiovascular Medicine, Graduate School of Medicine, University of Tokyo, Tokyo 113-8656, Japan

Edited by Gottfried Schatz, University of Basel, Reinach, Switzerland, and approved November 19, 2013 (received for review October 7, 2013)

The oxidative phosphorylation (OXPHOS) system generates most of the ATP in respiring cells. ATP-depleting conditions, such as hypoxia, trigger responses that promote ATP production. However, how OXPHOS is regulated during hypoxia has yet to be elucidated. In this study, selective measurement of intramitochondrial ATP levels identified the hypoxia-inducible protein G0/G1 switch gene 2 (G0s2) as a positive regulator of OXPHOS. A mitochondria-targeted, FRET-based ATP biosensor enabled us to assess OXPHOS activity in living cells. Mitochondria-targeted, FRET-based ATP biosensor and ATP production assay in a semi-intact cell system revealed that G0s2 increases mitochondrial ATP production. The expression of G0s2 was rapidly and transiently induced by hypoxic stimuli, and G0s2 interacts with OXPHOS complex V (F_oF_1-ATP synthase). Furthermore, physiological enhancement of G0s2 expression prevented cells from ATP depletion and induced a cellular tolerance for hypoxic stress. These results show that G0s2 positively regulates OXPHOS activity by interacting with F_oF_1-ATP synthase, which causes an increase in ATP production in response to hypoxic stress and protects cells from a critical energy crisis. These findings contribute to the understanding of a unique stress response to energy depletion. Additionally, this study shows the importance of assessing intramitochondrial ATP levels to evaluate OXPHOS activity in living cells.

energy metabolism | live-cell imaging

Maintaining cellular homeostasis and activities requires a stable energy supply. Most eukaryotic cells generate ATP as their energy currency mainly through the mitochondrial oxidative phosphorylation (OXPHOS) system. The OXPHOS system consists of five large protein complex units (i.e., complexes I–V), comprising more than 100 proteins. In this system, oxygen (O_2) is essential as the terminal electron acceptor for complex IV to finally produce the proton-motive force that drives the ATP-generating molecular motor complex V (F_oF_1-ATP synthase).

Hypoxia causes the depletion of intracellular ATP and triggers adaptive cellular responses to help maintain intracellular ATP levels and minimize any deleterious effects of energy depletion. Although the metabolic switch from mitochondrial respiration to anaerobic glycolysis is widely recognized (1–4), several recent reports have shown that hypoxic stimuli unexpectedly increase OXPHOS efficiency as well (5–7). In other words, cells have adaptive mechanisms to maintain intracellular ATP levels by enhancing OXPHOS, particularly in the early phase of hypoxia, in which the O_2 supply is limited but still remains. However, the mechanism by which OXPHOS is regulated during this early hypoxic phase is still not fully understood.

Revealing the mechanism of this fine-tuned regulation of OXPHOS requires accurate and noninvasive measurements of OXPHOS activity. Although researchers have established methods to measure OXPHOS activity, precise measurement, especially in living cells, is still difficult. Measuring the intracellular ATP concentration is one of the most commonly used methods for evaluating OXPHOS activity. However, there are two major problems with this method. First, the intracellular ATP concentration does not always accurately reflect OXPHOS activity, because it can also be affected by glycolytic ATP production, cytosolic ATPases, and ATP buffering enzymes, such as creatine kinase and adenylate kinase (8). Second, because measurements of the ATP concentration by chromatography (9), MS (10), NMR (11), or luciferase assays (12) are based on cell extract analysis, these methods cannot be used to measure the serial ATP concentration changes in living cells in real time.

In this study, we overcame these problems by the selective measurement of the intramitochondrial matrix ATP concentration ($[ATP]_{mito}$) in living cells. In the final step of OXPHOS, ATP is produced not in the cytosol but in the mitochondrial matrix. Therefore, we hypothesized that a selectively measuring $[ATP]_{mito}$ is suitable for the highly sensitive evaluation of cellular ATP production by OXPHOS. In fact, real-time evaluation of both $[ATP]_{mito}$ and the cytosolic ATP concentration ($[ATP]_{cyto}$) in living cells revealed that $[ATP]_{mito}$ reflected OXPHOS activity with far more sensitivity than $[ATP]_{cyto}$. Using this fine method, we found that G0/G1 switch gene 2 (G0s2), a hypoxia-induced

Significance

We developed a sensitive method to assess the activity of oxidative phosphorylation in living cells using a FRET-based ATP biosensor. We then revealed that G0/G1 switch gene 2, a protein rapidly induced by hypoxia, increases mitochondrial ATP production by interacting with F_oF_1-ATP synthase and protects cells from a critical energy crisis.

Author contributions: Y.A. and S.T. designed research; H. Kioka, H. Kato, O.T., and A.N. performed research; M.F., T.S., H.I., S.H., S.Y., T. Matsuzaki, K.T., H.A., M.A., T. Minamino, Y.S., M.Y., H.N., M.K., and I.K. contributed new reagents/analytic tools; H. Kioka and H. Kato analyzed data; and Y.A. and S.T. wrote the paper.

The authors declare no conflict of interest.

This article is a PNAS Direct Submission.

[1]H. Kioka and H. Kato contributed equally to this work.

[2]To whom correspondence may be addressed. E-mail: asano@cardiology.med.osaka-u.ac.jp or takasima@cardiology.med.osaka-u.ac.jp.

This article contains supporting information online at www.pnas.org/lookup/suppl/doi:10.1073/pnas.1318547111/-/DCSupplemental.

protein in cardiomyocytes, increases OXPHOS activity. G0s2 interacted with F_oF_1-ATP synthase and increased the ATP production rate. Our results suggest that hypoxia-induced protein G0s2 is a positive regulator of OXPHOS and protects cells by preserving ATP production, even under hypoxic conditions.

Results

Establishment of a Sensitive Method to Assess OXPHOS Activity in Living Cells. To elucidate the mechanism by which OXPHOS is regulated under hypoxia, it is essential to establish a sensitive method for assessing OXPHOS activity in living cells. For this purpose, we used an ATP indicator based on ε-subunit for analytical measurements (ATeam), which is an ATP-sensing FRET-based indicator (13). We introduced this ATP biosensor into cardiomyocytes that possess an abundance of mitochondria and produce the highest levels of ATP among all primary cells (14, 15). The ATeam assay can measure both $[ATP]_{cyto}$ (i.e., the Cyto-ATeam assay) and $[ATP]_{mito}$ when a duplex of the mitochondrial targeting signal of cytochrome *c* oxidase subunit VIII is attached to the indicator (i.e., the Mit-ATeam assay). In this case, the YFP/CFP emission ratio of the ATeam fluorescence represents the ATP concentration in each compartment. Interestingly, the Mit-ATeam assay was a far more sensitive method than the Cyto-ATeam assay in determining OXPHOS activity in living cells. For example, a very low dose of oligomycin A (0.01 μg/mL), a specific OXPHOS complex V (F_oF_1-ATP synthase) inhibitor, greatly reduced the YFP/CFP emission ratio of the Mit-ATeam fluorescence that represents $[ATP]_{mito}$ within 10 min (Fig. 1 *A*, *Upper* and *B* and Movie S1). In contrast, the same dose of oligomycin A resulted in a slight and slow decline of the YFP/CFP emission ratio of Cyto-ATeam fluorescence (Fig. 1 *A*, *Lower* and *B* and Movie S1). The same phenomenon was observed when the cells were exposed to hypoxia, which suppresses the activity of OXPHOS complex IV (cytochrome *c* oxidase). Again, $[ATP]_{mito}$ decreased more markedly than $[ATP]_{cyto}$ during 2.5 h of hypoxia (Fig. 1 *C* and *D* and Movie S2). These results indicate that the Mit-ATeam assay is far more sensitive for measuring the activity of OXPHOS than the Cyto-ATeam assay. In addition, OXPHOS inhibition decreased the YFP/CFP emission ratio of the Mit-ATeam fluorescence of HeLa cells as well as cardiomyocytes (Fig. S1), suggesting the broad applicability of this assay. Therefore, we used Mit-ATeam for the assessment of the OXPHOS activity in living cells.

Hypoxia-Induced Gene G0s2 Affects the Intramitochondrial ATP Concentration. The expression of genes involved in OXPHOS regulation is considered to be up-regulated in the early phase of hypoxia. Thus, to find unique OXPHOS regulators, we focused on the rapidly induced genes in response to hypoxic stimulation. We compared the gene expression profiles of cultured rat cardiomyocytes at three different time points during hypoxic conditions (0, 2, and 12 h) (Fig. S2*A*). The expression of well-known hypoxia-induced genes, such as VEGF-α and hexokinase 2 mRNA (16, 17), was slightly up-regulated at 2 h and further enhanced at 12 h of hypoxia. In contrast, three other genes (*Adamts1*, *Cdkn3*, and *G0s2*) underwent rapid increases in expression at 2 h but declined at 12 h of sustained hypoxia (Fig. S2 *B* and *C*). This rapid and transient time course of expression implies that these three genes may play distinct regulatory roles, especially in the early hypoxic phase, in which oxygen is limited but still available. To examine whether these genes are involved in the regulation of OXPHOS activity, we knocked down these genes by shRNA (see Fig. S7*A*) and examined $[ATP]_{mito}$ using the Mit-ATeam assay. In this experiment, $[ATP]_{mito}$ in cardiomyocytes treated with shRNA for G0s2 clearly declined within 24 h compared with the control cardiomyocytes (Fig. 2*A* and Movie S3). In addition, the time course of ATP decline was in agreement with the time course of G0s2 depletion (Fig. 2*A* and Fig. S3*A*). Importantly, the overexpression of G0s2 restored normal ATP levels (Fig. 2 *B* and *C*), and again, the Cyto-ATeam assay could not detect a significant effect of G0s2 knockdown within this time frame (Fig. S3*B* and Movie S4). These findings imply that mitochondrial ATP production through OXPHOS was inhibited by G0s2 ablation. We confirmed that the mRNA and protein levels of G0s2 both increased after 2–6 h of hypoxia and then declined after 12 h of hypoxia (Fig. 2 *D* and *E*). G0s2 was first reported as a gene with

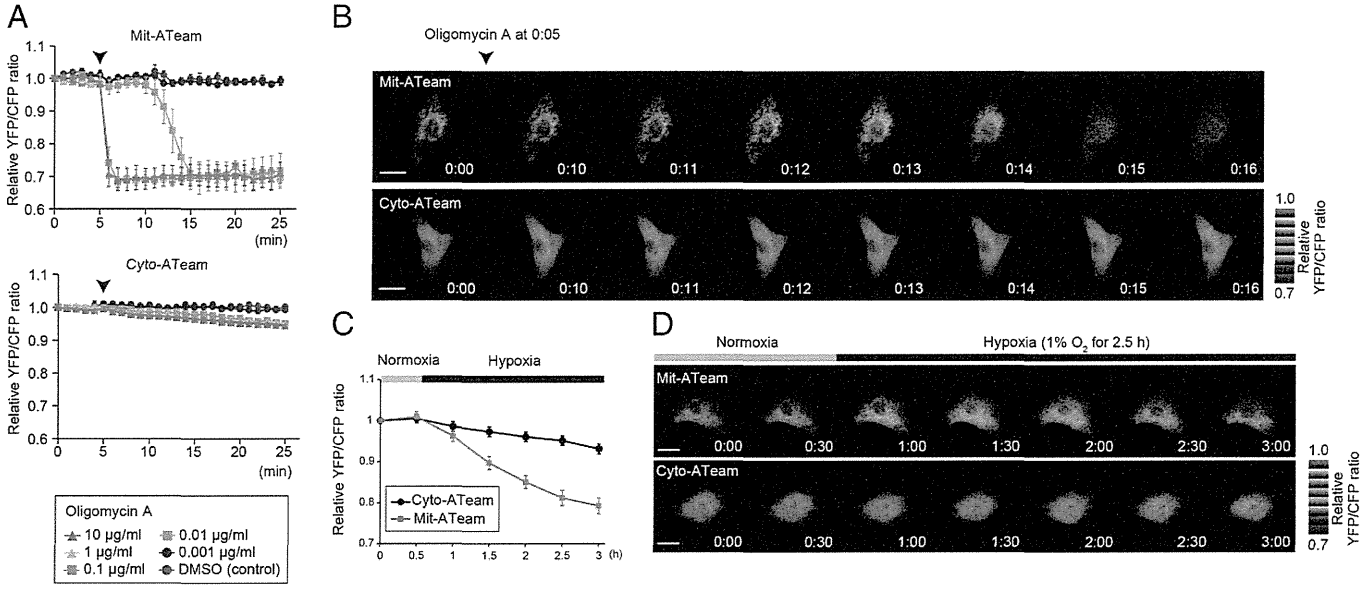

Fig. 1. Establishment of a sensitive method to assess OXPHOS activity in living cells. (*A*) YFP/CFP emission ratio plots of (*Upper*) Mit-ATeam and (*Lower*) Cyto-ATeam fluorescence in cardiomyocytes. Various concentrations (0.001, 0.01, 0.1, 1, and 10 μg/mL) of oligomycin A or DMSO (control) were added at 5 min (arrowhead; $n = 3$). (*B*) Representative sequential YFP/CFP ratiometric pseudocolored images of (*Upper*) Mit-ATeam and (*Lower*) Cyto-ATeam in cardiomyocytes. Oligomycin A (0.01 μg/mL) was added at 5 min. (Scale bars: 20 μm.) (*C*) YFP/CFP emission ratio plots of Mit-ATeam and Cyto-ATeam fluorescence in cardiomyocytes ($n = 10$). (*D*) Representative sequential YFP/CFP ratiometric pseudocolored images of (*Upper*) Mit-ATeam and (*Lower*) Cyto-ATeam in cardiomyocytes. Cells were exposed to 1% hypoxia from the time point 30 min. All of the measurements were normalized to the YFP/CFP emission ratio at 0 min. Data are represented as the means ± SEMs. (Scale bars: 20 μm.)

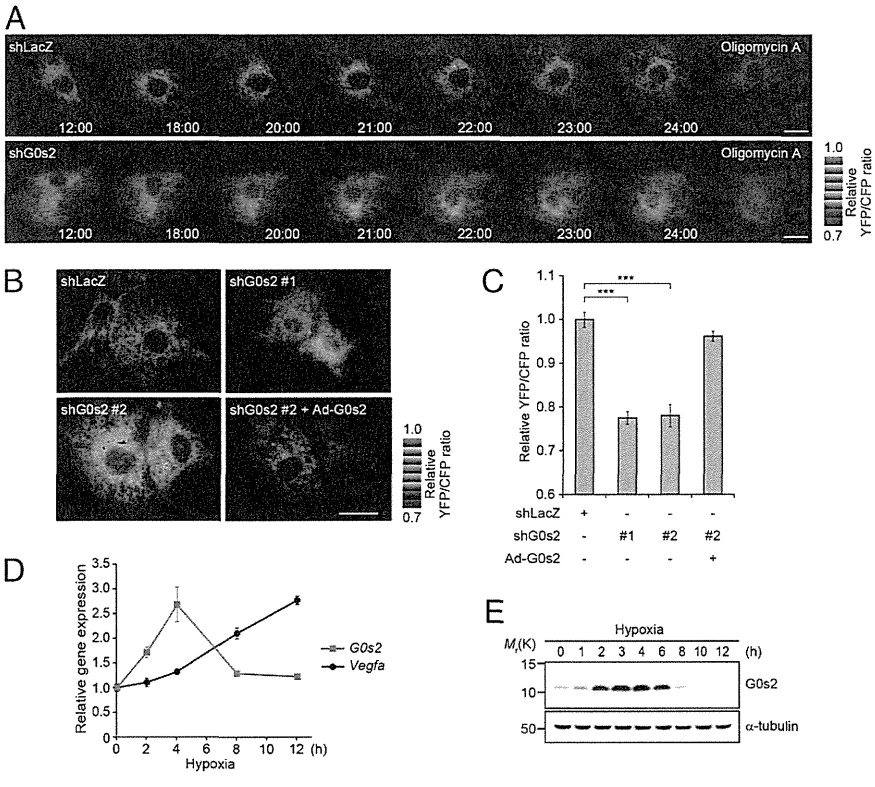

Fig. 2. G0s2, a hypoxia-inducible protein, affects intramitochondrial ATP concentration in cardiomyocytes. (*A*) Sequential YFP/CFP ratiometric pseudocolored images of Mit-ATeam fluorescence in cardiomyocytes expressing (*Upper*) shRNAs for LacZ (shLacZ) or (*Lower*) G0s2 (shG0s2). Oligomycin A (1 μg/mL) was added at the end of the time-lapse imaging to completely inhibit ATP synthesis. The indicated time represents the period after adenovirus infection. (*B*) Representative YFP/CFP ratiometric pseudocolored images of Mit-ATeam fluorescence in cardiomyocytes expressing the indicated adenovirus for 24 h. (Scale bar: *A* and *B*, 20 μm.) (*C*) The bar graph shows the mean YFP/CFP emission ratio of Mit-ATeam fluorescence in cardiomyocytes expressing shLacZ (n = 30), shG0s2 #1 (n = 30), shG0s2 #2 (n = 29), and shG0s2 #2 + G0s2 WT (n = 32) for 24 h. All of the measurements were normalized to the average of the control cells (shLacZ). ***$P < 0.001$. (*D*) Gene expression value plots of *G0s2* (red line) and *VEGF-α* (*Vegfa*; black line) levels in cardiomyocytes under hypoxic conditions (1% O_2). Each value was compared with the level of *Actb* expression (n = 3). Values represent the means ± SEMs. (*E*) Immunoblotting of the G0s2 expression in cardiomyocytes under hypoxic conditions (1% O_2).

expression that was induced during the cell cycle switch from G0 to G1 phase (18). G0s2 is expressed in many tissues and especially abundant in heart, skeletal muscle, liver, kidney, brain, and adipose tissue (19). Although G0s2 may play a role in cell cycle progression (20), the function of G0s2 in the hypoxic response remains unknown.

G0s2 Rescues the Decline of ATP Production During Hypoxia. We next tested whether the overexpression of the G0s2 before hypoxic stress could prevent hypoxia-induced ATP depletion. We prepared cardiomyocytes overexpressing G0s2 and control cardiomyocytes. During sustained hypoxia, $[ATP]_{mito}$ gradually declined in control cardiomyocytes as measured by the Mit-ATeam assay. Notably, the overexpression of G0s2 before the onset of hypoxia reduced this decline in $[ATP]_{mito}$, which allowed the cardiomyocytes to promptly recover to baseline levels of $[ATP]_{mito}$ after reoxygenation (Fig. 3 *A* and *B* and Movie S5). In addition, the prehypoxia overexpression of G0s2 preserved cell viability during sustained hypoxia (Fig. 3*C*). These results suggest that G0s2 can preserve mitochondrial ATP production even under hypoxia and protect cells from the energy crisis under hypoxia.

G0s2 Binds to F_oF_1-ATP Synthase but Not Other OXPHOS Protein Complexes. To reveal the mechanism by which G0s2 affects $[ATP]_{mito}$, we sought to identify the biochemical targets of G0s2. We screened for G0s2 binding proteins by immunoaffinity purification of cell lysates from cardiomyocytes expressing C-terminally Flag-tagged G0s2 (G0s2-Flag). G0s2-Flag is expressed in cardiomyocytes localized to the mitochondria (Fig. S4*A*). MS analysis revealed that multiple F_oF_1-ATP synthase subunits, but no other mitochondrial respiratory chain complex subunits, were coimmunoprecipitated with G0s2-Flag (Fig. S4*B* and Table S1). F_oF_1-ATP synthase is a well-known ATP-producing enzyme composed of a protein complex that contains an extramembranous F_1 and an intramembranous F_o domain linked by a peripheral and a central stalk (21–24). The binding of F_oF_1-ATP synthase to G0s2-Flag was confirmed by immunoblotting with antibodies against several subunits of F_oF_1-ATP synthase (Fig. 4*A*).

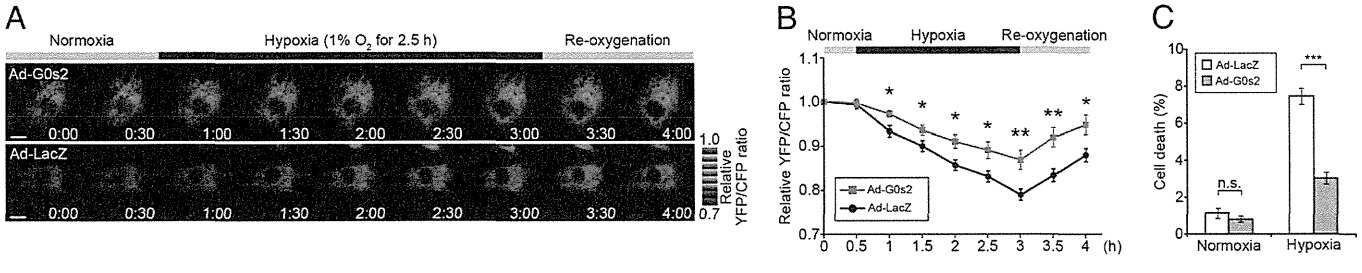

Fig. 3. Overexpression of G0s2 before hypoxia rescues the decline of mitochondrial ATP production during hypoxia. (*A*) Sequential YFP/CFP ratiometric pseudocolored images of Mit-ATeam fluorescence in cardiomyocytes expressing (*Upper*) G0s2 WT or (*Lower*) LacZ during hypoxia and reoxygenation. (Scale bar: 20 μm.) (*B*) YFP/CFP emission ratio plots of Mit-ATeam fluorescence in cardiomyocytes expressing G0s2 WT (n = 20) or LacZ (n = 19) during hypoxia and reoxygenation. All of the measurements were normalized to the ratio at time 0 and compared between cardiomyocytes with G0s2 WT and LacZ at each time point. (*C*) The bar graph shows the cell viability of cardiomyocytes overexpressing G0s2 under hypoxic conditions. Cardiomyocytes expressing either LacZ or G0s2 WT were cultured under normoxic or hypoxic conditions for 18 h (n = 8). The asterisks denote statistical significance comparing G0s2 with LacZ. Data are represented as the means ± SEMs. n.s., not significant. *$P < 0.05$; **$P < 0.01$; ***$P < 0.001$.

Conversely, G0s2-Flag was coimmunoprecipitated with F_oF_1-ATP synthase (Fig. S4*C*). G0s2-Flag was also found to be associated with the F_oF_1-ATP synthase in 293T and HeLa cells (Fig. S4*C*). Both coimmunoprecipitation using an anti-G0s2 antibody and a reciprocal immunoprecipitation revealed that endogenous G0s2 interacts with F_oF_1-ATP synthase, whereas none of the proteins in complexes I–IV or adenine nucleotide translocase 1 (ANT1; also referred to as ADP/ATP carrier) were coimmunoprecipitated with G0s2 (Fig. 4 *B* and *C*).

Given that the G0s2 protein contains an evolutionarily conserved amino terminus and one hydrophobic domain (HD) (19), we created three G0s2 partial deletion mutants to identify the domain in G0s2 that is important for binding to F_oF_1-ATP synthase (Fig. S4*D*). Among these mutants, G0s2 ΔC and G0s2 ΔN but not G0s2 ΔHD bound to the F_oF_1-ATP synthase complex (Fig. 4*D* and Fig. S4 *E* and *F*). Furthermore, we confirmed that G0s2 directly interacts with F_oF_1-ATP synthase in an in vitro pull-down assay using a recombinant maltose-binding protein–fused G0s2 protein and purified F_oF_1-ATP synthase from bovine heart mitochondria (Fig. S5). Immunocytochemical analysis revealed that endogenous G0s2 colocalized with the β-subunit of F_oF_1-ATP synthase (Fig. 4*E*). The knockdown of G0s2 expression by shRNA abolished G0s2 staining (Figs. S6 and S7*A*), indicating that both antibodies used for immunostaining specifically recognize G0s2. These data suggest that G0s2 interacts with the F_oF_1-ATP synthase complex through its HD in mitochondria and regulates OXPHOS activity.

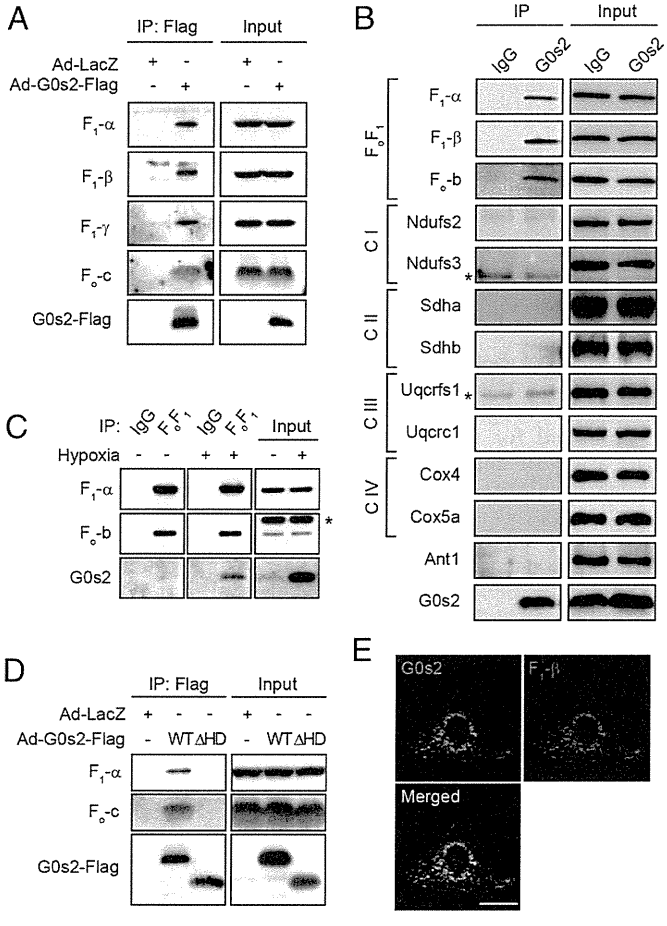

Fig. 4. G0s2 interacts with the F_oF_1-ATP synthase in mitochondria. (*A*) Immunoprecipitation (IP) of G0s2-Flag in cardiomyocytes. Cell lysates from cardiomyocytes expressing G0s2-Flag or LacZ were immunoprecipitated with an anti-Flag antibody. (*B*) IP of endogenous G0s2 in cardiomyocytes. Endogenous G0s2 was induced by hypoxia and immunoprecipitated using an anti-G0s2 antibody. C, OXPHOS complex; F_oF_1, F_oF_1-ATP synthase. *IgG light chain. (*C*) IP of F_oF_1-ATP synthase in cardiomyocytes under normoxic or hypoxic conditions. Cell lysates from cardiomyocytes cultured under normoxia or hypoxia for 4 h were immunoprecipitated with an antibody against the whole F_oF_1-ATP synthase complex or a control IgG. *Nonspecific band. (*D*) IP of G0s2 mutants expressed in cardiomyocytes. Cell lysates were immunoprecipitated with an anti-Flag antibody. (*E*) Immunostained images of hypoxia-stimulated (4 h) cardiomyocytes with anti-G0s2 (green) and anti–F_oF_1-ATP synthase β-subunit (red) antibodies. (Scale bars: 20 μm.)

G0s2 Increases Mitochondrial ATP Production Rate. $[ATP]_{mito}$ is mainly determined by the rate of ATP synthesis by F_oF_1-ATP synthase and ATP/ADP exchange by the ATP/ADP translocase ANT1. This theory means that the increased $[ATP]_{mito}$ observed in the G0s2-overexpressing cells may result from the increased ATP synthesis and/or decreased ATP/ADP exchange, although G0s2 did not interact with ANT1 (Fig. 4*B*). To resolve this issue and directly measure the rate of ATP production in mitochondria, we used a semiintact cell system called the mitochondrial activity of streptolysin O permeabilized cells (MASC) assay (25). In this assay, we permeabilized the plasma membrane to wash out any cytosolic components, such as creatine and glycolytic substrates, but left the mitochondria intact. Furthermore, we treated the cells with P^1, P^5-di(adenosine-5′) pentaphosphate to inhibit the activity of adenylate kinase. These steps allowed us to measure the ATP production rate mostly from OXPHOS, with a minimal contribution of ATP buffering systems in the cytosol. The MASC assay was suitable for accurate measurement of mitochondrial ATP production rate, because mitochondria in this semiintact cell system suffered much smaller damage than the isolated mitochondria in the conventional method. Surprisingly, in the MASC assay, the ATP production rate markedly increased when G0s2 was expressed in HeLa cells that lacked endogenous G0s2 (Fig. 5*A*). In cardiomyocytes, shRNA-mediated G0s2 knockdown decreased the ATP production rate in mitochondria, and the expression of G0s2 WT but not G0s2 ΔHD could restore the ATP production rate (Fig. 5*B* and Fig. S7*A*). In both cells, complete inhibition of ATP production by oligomycin A indicated that the observed ATP synthesis was catalyzed by OXPHOS but not other metabolism (Fig. 5 *A* and *B*).

Next, to evaluate the physiological role of G0s2, we examined whether endogenous G0s2 induced by hypoxia could enhance the ATP production rate. Cardiomyocytes were pretreated with hypoxia for 4 h, during which G0s2 expression was largely induced. We then evaluated the ATP production rate of both hypoxia-pretreated and nontreated cardiomyocytes under room air conditions. Even under these equivalent normoxic conditions, hypoxia-pretreated cardiomyocytes produced ATP faster than nontreated control cardiomyocytes (Fig. 5*C* and Fig. S7*B*). G0s2 knockdown attenuated this increase in the rate of ATP production, indicating that the enhanced ATP production rate resulting from hypoxia pretreatment primarily depends on endogenous G0s2 induction. This increased G0s2 expression was essential for cell survival, because G0s2-depleted cells died earlier than control cells under conditions of hypoxic stress (Fig. 5*D*)

Furthermore, to assess the effect of G0s2 on cellular respiration, we continuously measured the oxygen consumption rate (OCR) using an XF96 Extracellular Flux Analyzer. G0s2 knockdown decreased the basal OCR of cardiomyocytes, most likely because of the decreased activity of ATP synthesis (Fig. 5 *E* and *F*). In contrast, the proton leakage of the mitochondrial inner membrane and the maximum respiratory capacity of OXPHOS complexes I–IV were unaffected by G0s2 ablation (Fig. 5 *E* and *F*). These data show that G0s2 knockdown reduced respiration caused by ATP synthesis without affecting respiration caused by proton leakage, nonmitochondrial respiration, or the maximal respiration capacity.

All these findings indicate that G0s2 enhances the mitochondrial ATP production rate by increasing the activity of F_oF_1-ATP synthase.

Discussion

In this study, we showed that G0s2 kinetically increased OXPHOS activity through direct binding to F_oF_1-ATP synthase. Our previous

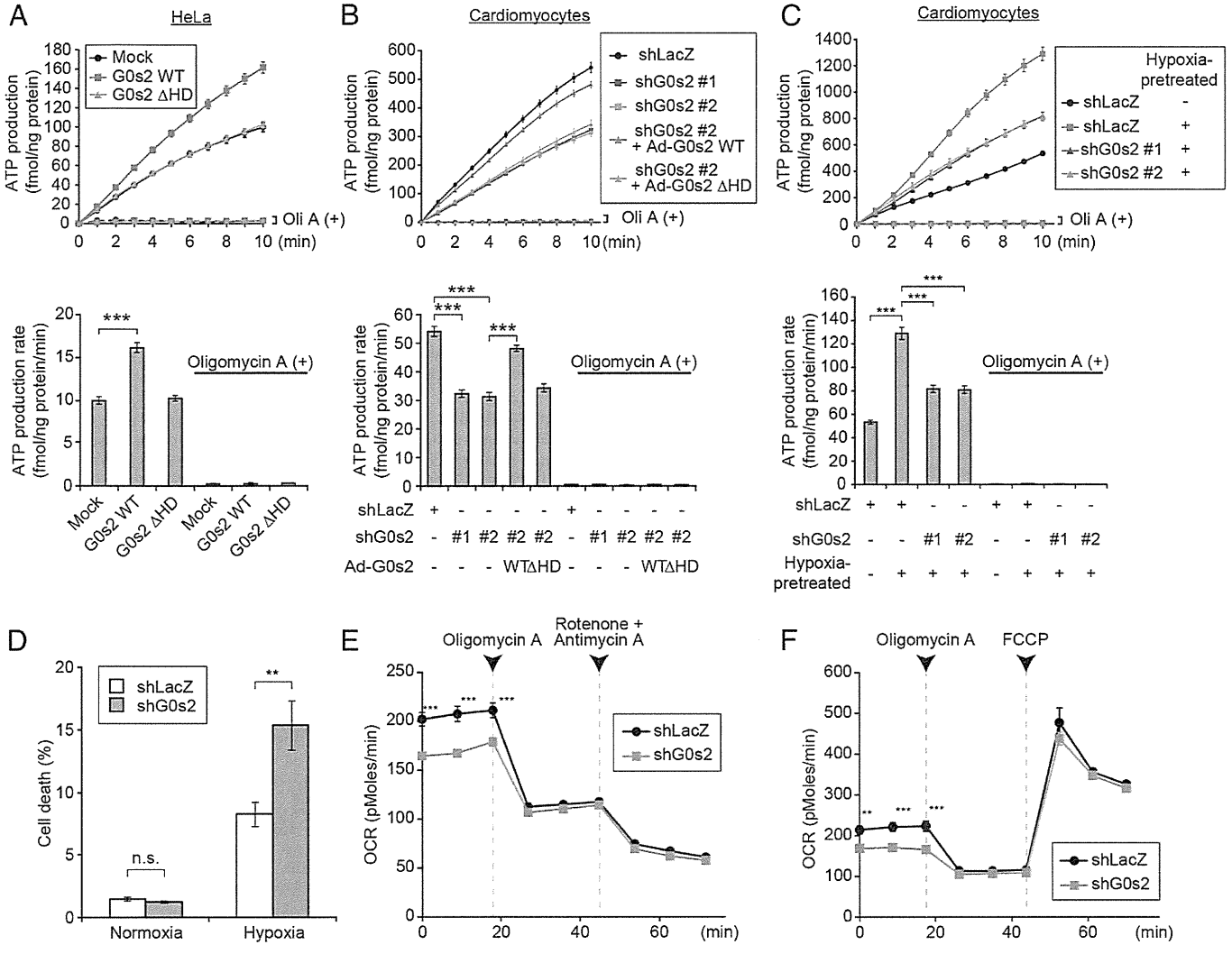

Fig. 5. G0s2 enhances the mitochondrial ATP production rate. (*A* and *B*) MASC assay of (*A*) permeabilized HeLa cells expressing the indicated plasmids or (*B*) cardiomyocytes expressing the indicated adenovirus in the presence (dotted lines) or absence (solid lines) of 1 μg/mL oligomycin A (Oli A). *Upper* shows the ATP production plots, and *Lower* shows the mean ATP production rates between 0 and 10 min. (*A*) $n = 12$. (*B*) Solid lines, $n = 12$; dotted lines, $n = 8$. (*C*) MASC assay of permeabilized cardiomyocytes pretreated with hypoxia. Cells expressing the indicated adenovirus were pretreated with or without hypoxia for 4 h. After the pretreatment, the cells were permeabilized under room air conditions followed by MASC assay in the presence (dotted lines; $n = 8$) or absence (solid lines; $n = 12$) of 1 μg/mL Oli A. *Upper* shows the ATP production plot, and *Lower* shows the mean ATP production rate between 0 and 10 min. (*D*) The bar graph represents the cell viability of G0s2-depleted cardiomyocytes under hypoxic conditions. Cardiomyocytes expressing shLacZ or shG0s2 (#2) were cultured under normoxic or hypoxic conditions for 18 h. (*E* and *F*) The OCR in cardiomyocytes expressing shLacZ and shG0s2 (#2) under basal conditions and in response to the indicated mitochondrial inhibitors ($n = 8$). FCCP, carbonyl cyanide-4-(trifluoromethoxy)-phenylhydrazone. Data are represented as the means ± SEMs. n.s., not significant. $^{**}P < 0.01$; $^{***}P < 0.001$.

studies of F_oF_1-ATP synthase have revealed that this enzyme has a specific structure that connects two molecular nanomotors that synchronize with each other to produce ATP (26–30). These physically distinct structures suggest that a specific activating factor for F_oF_1-ATP synthase must exist. Combined with the findings from this study, we hypothesize that G0s2 may lower the activation barrier of the F_oF_1-ATP synthase nanomotor and enhance the ATP production rate with the equivalent proton motive driving force (PMF; i.e., the sum of the membrane potential and the pH gradient). Activation barriers might be generated by various factors, such as friction between the stator and rotor of F_oF_1-ATP synthase, physical and electrical resistance to proton transport through the channel, and the existence of rotary blockers such as the bacterial ε-subunit and cyclophilin D (31). The increased ATP production rate caused by G0s2 overexpression observed in the MASC assay supports this hypothesis, because the PMF in the initial phase of this assay should be the same. If this hypothesis is true, even with reduced PMF, cells that express G0s2 should produce ATP faster than cells that express little or no G0s2. In fact, G0s2 overexpression attenuated the decline of $[ATP]_{mito}$ under hypoxic conditions that reduced the PMF. Precise real-time measurement of the PMF is currently difficult, but these hypotheses might be proven in future studies. Kinetically faster ATP production should accompany greater consumption of both O_2 and PMF; however, our results suggest that preserving ATP production is more beneficial than preserving PMF for cell viability, particularly when the O_2 supply is restricted but still exists. The transience of endogenous G0s2 expression induced by hypoxia might serve to protect tissues in the early phase of energy crisis. There may be specific mechanisms to decrease G0s2 expression under prolonged ischemia that have yet to be identified. Another possible mechanism by which G0s2 could increase the ATP production rate is that G0s2 increases the F_o-F_1 coupling efficiency of F_oF_1-ATP synthase. However, this hypothesis is less likely, because G0s2 altered the oxygen consumption rate to increase the ATP production rate. Although this uncoupling phenomenon has rarely been reported for mammalian mitochondrial F_oF_1-ATP synthase, we cannot completely eliminate the possibility that intrinsically

uncoupled F_oF_1-ATP synthase exists, because we could not accurately measure the amount of uncoupled F_oF_1-ATP synthase in intact cells.

G0s2 was first identified in cultured monocytes during the drug-induced cell cycle transition from G0 to G1 phase (18, 32). A limited number of studies have implied that G0s2 is involved in cell proliferation (33), differentiation (19), apoptosis (34), inflammation (35), and lipid metabolism (36) in various cellular settings. Moreover, G0s2 was reported to localize to the cytosol (33), endoplasmic reticulum (19), mitochondria (34), or the surface of lipid droplets (36). How G0s2 distinguishes these multiple functions is still not clear. In our hands, G0s2 is always localized to mitochondria, which was shown by immunostaining with two antibodies against different epitopes of G0s2 (Fig. S6). Complete depletion of mitochondrial staining by G0s2 knockdown strongly suggests the specific localization of G0s2 to mitochondria. We also showed that G0s2 specifically bound to mitochondrial F_oF_1-ATP synthase but not other OXPHOS protein complexes and functionally regulated OXPHOS activity. Together, these data suggest that G0s2 acts in the mitochondria. However, different cellular conditions may change the localization and role of G0s2. Additionally, G0s2-mediated changes in ATP metabolism may possibly affect the lipid metabolism or cellular proliferation. Additional studies will reveal the functional mechanisms by which G0s2 exerts these multiple functions in different cellular conditions.

In this study, we evaluated $[ATP]_{mito}$ and $[ATP]_{cyto}$ separately using FRET-based ATP biosensors in living cells. This dual evaluation revealed that $[ATP]_{mito}$ reflected mitochondrial ATP production with much greater sensitivity than $[ATP]_{cyto}$ (Fig. 1 and Movies S1 and S2). Because $[ATP]_{cyto}$ is strongly influenced by the activity of various cytosolic ATP hydrolytic enzymes and ATP buffering enzymes, $[ATP]_{cyto}$ does not always reflect the ATP availability that determines cellular function.

Taken together, our results indicate that G0s2 is a positive regulator of OXPHOS that works to increase the mitochondrial ATP production rate even under hypoxic conditions. Therefore, enhancing the level and function of G0s2 could be beneficial for hypoxia- and mitochondria-related disorders, such as ischemic diseases, metabolic diseases, and cancer.

Materials and Methods

Cells were infected with adenovirus encoding FRET-based ATP indicators AT1.03 or mit-AT1.03 to measure changes in cytosolic or mitochondrial ATP concentrations, respectively. Image acquisitions and FRET analyses were performed as described previously with some modifications (13). For the control of oxygen concentration during time-lapse imaging, digital gas mixer for stage-top incubator GM8000 (Tokai Hit) was used to create hypoxic (1% O_2) or normoxic (20% O_2) condition. Additional methods are found in *SI Materials and Methods*.

ACKNOWLEDGMENTS. We thank M. Murata for helpful discussions and advice, H. Miyagi (Olympus Co. Ltd.) for technical advice regarding microscopy, T. Miyazaki (Cyclex Co. Ltd.) for making antibodies, S. Ikezawa and A. Ogai for technical assistance, K. Tanaka for help with the purification of bovine F_oF_1-ATP synthase, and Y. Okada and H. Fujii for secretarial support. This research was supported by the Japan Society for the Promotion of Science through the Funding Program for Next Generation World-Leading Researchers (NEXT Program) initiated by the Council for Science and Technology Policy; grants-in-aid from the Ministry of Health, Labor, and Welfare–Japan; and grants-in-aid from the Ministry of Education, Culture, Sports, Science, and Technology–Japan. This research was also supported by grants from Takeda Science Foundation, Japan Heart Foundation, Japan Cardiovascular Research Foundation, Japan Intractable Diseases Research Foundation, Japan Foundation of Applied Enzymology, Japan Medical Association, Uehara Memorial Foundation, Mochida Memorial Foundation, Banyu Foundation, Naito Foundation, Inoue Foundation for Science, Osaka Medical Research foundation for Intractable Diseases, Ichiro Kanehara Foundation, and Showa Houkoukai.

1. Kim JW, Tchernyshyov I, Semenza GL, Dang CV (2006) HIF-1-mediated expression of pyruvate dehydrogenase kinase: A metabolic switch required for cellular adaptation to hypoxia. *Cell Metab* 3(3):177–185.
2. Papandreou I, Cairns RA, Fontana L, Lim AL, Denko NC (2006) HIF-1 mediates adaptation to hypoxia by actively downregulating mitochondrial oxygen consumption. *Cell Metab* 3(3): 187–197.
3. Semenza GL (2012) Hypoxia-inducible factors in physiology and medicine. *Cell* 148(3): 399–408.
4. Semenza GL, et al. (1996) Hypoxia response elements in the aldolase A, enolase 1, and lactate dehydrogenase A gene promoters contain essential binding sites for hypoxia-inducible factor 1. *J Biol Chem* 271(51):32529–32537.
5. Chen YC, et al. (2012) Identification of a protein mediating respiratory supercomplex stability. *Cell Metab* 15(3):348–360.
6. Fukuda R, et al. (2007) HIF-1 regulates cytochrome oxidase subunits to optimize efficiency of respiration in hypoxic cells. *Cell* 129(1):111–122.
7. Strogolova V, Furness A, Robb-McGrath M, Garlich J, Stuart RA (2012) Rcf1 and Rcf2, members of the hypoxia-induced gene 1 protein family, are critical components of the mitochondrial cytochrome bc1-cytochrome c oxidase supercomplex. *Mol Cell Biol* 32(8):1363–1373.
8. Saks V, et al. (2006) Cardiac system bioenergetics: Metabolic basis of the Frank-Starling law. *J Physiol* 571(Pt 2):253–273.
9. Smolenski RT, Lachno DR, Ledingham SJ, Yacoub MH (1990) Determination of sixteen nucleotides, nucleosides and bases using high-performance liquid chromatography and its application to the study of purine metabolism in hearts for transplantation. *J Chromatogr A* 527(2):414–420.
10. Shimura D, et al. (2013) Metabolomic profiling analysis reveals chamber-dependent metabolite patterns in the mouse heart. *Am J Physiol Heart Circ Physiol* 305(4):H494–H505.
11. Kemp GJ, Meyerspeer M, Moser E (2007) Absolute quantification of phosphorus metabolite concentrations in human muscle in vivo by 31P MRS: A quantitative review. *NMR Biomed* 20(6):555–565.
12. Ford SR, et al. (1996) Use of firefly luciferase for ATP measurement: Other nucleotides enhance turnover. *J Biolumin Chemilumin* 11(3):149–167.
13. Imamura H, et al. (2009) Visualization of ATP levels inside single living cells with fluorescence resonance energy transfer-based genetically encoded indicators. *Proc Natl Acad Sci USA* 106(37):15651–15656.
14. Lopaschuk GD, Kelly DP (2008) Signalling in cardiac metabolism. *Cardiovasc Res* 79(2): 205–207.
15. Hattori F, et al. (2010) Nongenetic method for purifying stem cell-derived cardiomyocytes. *Nat Methods* 7(1):61–66.
16. Forsythe JA, et al. (1996) Activation of vascular endothelial growth factor gene transcription by hypoxia-inducible factor 1. *Mol Cell Biol* 16(9):4604–4613.
17. Wolf A, et al. (2011) Hexokinase 2 is a key mediator of aerobic glycolysis and promotes tumor growth in human glioblastoma multiforme. *J Exp Med* 208(2):313–326.
18. Russell L, Forsdyke DR (1991) A human putative lymphocyte G0/G1 switch gene containing a CpG-rich island encodes a small basic protein with the potential to be phosphorylated. *DNA Cell Biol* 10(8):581–591.
19. Zandbergen F, et al. (2005) The G0/G1 switch gene 2 is a novel PPAR target gene. *Biochem J* 392(Pt 2):313–324.
20. Heckmann BL, Zhang X, Xie X, Liu J (2013) The G0/G1 switch gene 2 (G0S2): Regulating metabolism and beyond. *Biochim Biophys Acta* 1831(2):276–281.
21. Dimroth P, von Ballmoos C, Meier T (2006) Catalytic and mechanical cycles in F-ATP synthases. Fourth in the Cycles Review Series. *EMBO Rep* 7(3):276–282.
22. Senior AE (2007) ATP synthase: Motoring to the finish line. *Cell* 130(2):220–221.
23. Walker JE (1998) ATP synthesis by rotary catalysis (Nobel Lecture). *Angew Chem Int Ed* 37:5000–5011.
24. Yoshida M, Muneyuki E, Hisabori T (2001) ATP synthase—a marvellous rotary engine of the cell. *Nat Rev Mol Cell Biol* 2(9):669–677.
25. Fujikawa M, Yoshida M (2010) A sensitive, simple assay of mitochondrial ATP synthesis of cultured mammalian cells suitable for high-throughput analysis. *Biochem Biophys Res Commun* 401(4):538–543.
26. Adachi K, et al. (2007) Coupling of rotation and catalysis in F(1)-ATPase revealed by single-molecule imaging and manipulation. *Cell* 130(2):309–321.
27. Itoh H, et al. (2004) Mechanically driven ATP synthesis by F1-ATPase. *Nature* 427(6973):465–468.
28. Noji H, Yasuda R, Yoshida M, Kinosita K, Jr. (1997) Direct observation of the rotation of F1-ATPase. *Nature* 386(6622):299–302.
29. Rondelez Y, et al. (2005) Highly coupled ATP synthesis by F1-ATPase single molecules. *Nature* 433(7027):773–777.
30. Uchihashi T, Iino R, Ando T, Noji H (2011) High-speed atomic force microscopy reveals rotary catalysis of rotorless F_1-ATPase. *Science* 333(6043):755–758.
31. Giorgio V, et al. (2009) Cyclophilin D modulates mitochondrial F0F1-ATP synthase by interacting with the lateral stalk of the complex. *J Biol Chem* 284(49):33982–33988.
32. Siderovski DP, Blum S, Forsdyke RE, Forsdyke DR (1990) A set of human putative lymphocyte G0/G1 switch genes includes genes homologous to rodent cytokine and zinc finger protein-encoding genes. *DNA Cell Biol* 9(8):579–587.
33. Yamada T, Park CS, Burns A, Nakada D, Lacorazza HD (2012) The cytosolic protein G0S2 maintains quiescence in hematopoietic stem cells. *PLoS ONE* 7(5):e38280.
34. Welch C, et al. (2009) Identification of a protein, G0S2, that lacks Bcl-2 homology domains and interacts with and antagonizes Bcl-2. *Cancer Res* 69(17):6782–6789.
35. Kobayashi S, et al. (2008) Expression profiling of PBMC-based diagnostic gene markers isolated from vasculitis patients. *DNA Res* 15(4):253–265.
36. Yang X, et al. (2010) The G(0)/G(1) switch gene 2 regulates adipose lipolysis through association with adipose triglyceride lipase. *Cell Metab* 11(3):194–205.

Atherosclerosis 227 (2013) 373–379

Contents lists available at SciVerse ScienceDirect

Atherosclerosis

journal homepage: www.elsevier.com/locate/atherosclerosis

Decreased mortality associated with statin treatment in patients with acute myocardial infarction and lymphotoxin-alpha C804A polymorphism

Shinichiro Suna [a,1], Yasuhiko Sakata [a,b,*,1], Daisaku Nakatani [a,1], Keiji Okuda [a,1], Masahiko Shimizu [a,1], Masaya Usami [a,1], Sen Matsumoto [a,1], Masahiko Hara [a,1], Kouichi Ozaki [c,1], Hiroya Mizuno [a,1], Tetsuo Minamino [a,1], Seiji Takashima [a,1], Masami Nishino [d,1], Yasushi Matsumura [e,1], Hiroshi Takeda [e,1], Toshihiro Tanaka [c,1], Hiroshi Sato [f,1], Masatsugu Hori [g,1], Issei Komuro [a,1]

[a] Department of Cardiovascular Medicine, Osaka University Graduate School of Medicine, Suita, Japan
[b] Department of Evidence-Based Cardiovascular Medicine, Tohoku University Graduate School of Medicine, Sendai, Japan
[c] Laboratory for Cardiovascular Diseases, SNP Research Center, RIKEN Center for Genomic Medicine, Yokohama, Japan
[d] Osaka Rosai Hospital, Sakai, Japan
[e] Department of Medical Information Science, Osaka University Graduate School of Medicine, Suita, Japan
[f] School of Human Welfare Studies, Kwansei Gakuin University, Nishinomiya, Japan
[g] Osaka Medical Center for Cancer and Cardiovascular Disease, Osaka, Japan

ARTICLE INFO

Article history:
Received 23 August 2012
Received in revised form
11 January 2013
Accepted 14 January 2013
Available online 25 January 2013

Keywords:
Lymphotoxin alpha
Myocardial infarction
Single nucleotide polymorphism
Statin

ABSTRACT

Aims: We previously reported the association of single nucleotide polymorphisms in the lymphotoxin alpha (LTα) gene with susceptibility to acute myocardial infarction (AMI) and increased mortality after discharge. In the present study, we investigated whether the adverse effect of LTα C804A polymorphism on mortality could be pharmacologically modified by statin treatment after AMI.

Methods and results: We conducted a multicenter study that included 3486 post-AMI patients between 1998 and 2008. During a median follow-up period of 1775 days, 247 deaths were recorded. The mortality rate was significantly higher in LTα 804A allele carriers compared to non-804A allele carriers (7.9% vs. 5.7%, $p = 0.011$). The LTα 804A allele was significantly associated with increased mortality for post-AMI patients not receiving statins (hazard ratio [HR]: 1.48, 95% confidence interval [CI]: 1.03–2.12, $p = 0.034$), but not for those receiving statins (HR: 1.22, 95% CI: 0.70–2.10, $p = 0.486$). *In-vitro* experimental analyses demonstrated that the LTα 804A polymorphic protein, 26Asn-LTα_3, induced monocyte-endothelial interaction and endoplasmic reticulum (ER) stress in cardiomyocytes more strongly than the LTα_3 804C polymorphic protein 26Thr-LTα_3. However, the effects of both LTα_3 proteins were decreased and became comparable by the pretreatment of cells with pravastatin.

Conclusion: LTα C804A polymorphism was associated with an increased risk of mortality for AMI patients, although this effect was masked in patients treated with statins. This finding is supported by the observed attenuation of 26Asn-LTα_3-mediated monocyte-endothelial interaction and ER stress in cardiomyocytes treated with pravastatin. LTα C804A polymorphism may have potential as a novel therapeutic target for secondary prevention after AMI.

1. Introduction

Myocardial infarction (MI) is one of the major causes of death in developed countries. Although the implementation of evidence-based therapies has greatly reduced mortality [1,2], the long-term mortality rate after discharge for AMI remains high. Because personal risk after AMI survival dramatically varies demographically, the development of improved secondary prevention programs,

Abbreviations: AMI, acute myocardial infarction; Asn, asparagine; CI, confidence interval; ER, endoplasmic reticulum; GRP, glucose-regulated protein; HR, hazard ratio; HUVEC, human umbilical vein endothelial cells; LTα, lymphotoxin alpha; SNPs, single nucleotide polymorphisms; Thr, threonine; TNF, tumor necrosis factor; VCAM1, vascular cell adhesion molecules 1.

* Corresponding author. Department of Evidence-based Cardiovascular Medicine, Tohoku University Graduate School of Medicine, 1-1 Seiryo-machi, Aoba-ku, Sendai 980-8574, Japan. Tel.: +81 22 717 7152; fax: +81 22 717 7156.
E-mail address: sakatayk@cardio.med.tohoku.ac.jp (Y. Sakata).

[1] On behalf of the Osaka Acute Coronary Insufficiency Study.

0021-9150/$ – see front matter © 2013 Elsevier Ireland Ltd. All rights reserved.
http://dx.doi.org/10.1016/j.atherosclerosis.2013.01.020

including personalized therapy approaches is necessary to reduce post-AMI mortality. In particular, therapeutic approaches that take into account genetically determined risk may have great potential for personalized treatments that improve adverse outcomes after MI.

Recently, others and we identified that single nucleotide polymorphisms (SNPs) in the genes encoding lymphotoxin alpha (LTα) and its associated proteins are associated with AMI onset [3–8]. LTα is a proinflammatory cytokine with homology to inflammatory cytokine tumor necrosis factor (TNF)-α [9–11] and is related with the development of atherosclerotic lesions in coronary arteries [12,13]. Interestingly, SNPs in the LTα gene are associated with both increased susceptibility to AMI onset post-AMI mortality [14]. Based on the pro-inflammatory characteristics of LTα, we hypothesized that the adverse effects of LTα polymorphism could be mediated by statins, which are one of the most widely prescribed medicines with anti-inflammatory properties [15].

Here, we investigated the pharmacogenetic interactions between LTα C804A polymorphism and statins in post-AMI patients, and attempted to determine the underlying mechanisms through *in-vitro* analyses.

2. Materials and methods

2.1. Epidemiologic data regarding the impact of LTα C804A polymorphism

Among 10,076 consecutive Japanese AMI patients who were registered in the Osaka Acute Coronary Insufficiency Study (OACIS) between 1998 and 2008, we enrolled 3486 patients who were discharged alive and submitted samples for the genetic analysis performed in this study. Details of the OACIS and genotyping have been reported elsewhere [14,16]. All patients provided written informed consent, and the study protocol complied with the Guidelines for Genome/Genetic Research issued by the Japanese government and was approved by the ethics committee of each institution.

The patients were divided into two groups according to the presence (n = 1390; statin(+) group) or absence (n = 2096; statin(−) group) of statin treatment at discharge. In each group, the incidence of all-cause mortality was compared between patients with the AA or CA genotype (A allele carriers) and those with the CC genotype (non-A allele carriers) of LTα C804A polymorphism. LTα C804A polymorphism (rs1041981) was determined using an automated fluorescent allele-specific DNA primer assay (Toyobo Gene Analysis, Tsuruga, Japan) [17].

2.2. Cell culture and materials

Human umbilical vein endothelial cells (HUVEC) were purchased from Clonetics (San Diego, CA, USA) and cultured in EGM-2 SingleQuots endothelial cell medium (Clonetics) at 37 °C in a humidified 5% CO_2 incubator. Cells from passages three to eight were used for experiments. THP1 cells, a human acute monocytic leukemia cell line, were purchased from ATCC (Manassas, VA, USA) and cultured in RPMI 1640 medium (Clonetics) containing 10% fetal calf serum, 2 μM glutamine, and 1% penicillin/streptomycin at 37 °C in a humidified 5% CO_2 incubator [12]. Recombinant 26Thr-LTα_3 and 26Asn-LTα_3 proteins were expressed in *Escherichia coli* using the pET29 system (Novagen, Madison, WI, USA) and purified as previously described [8]. Cytotoxic assays were conducted in the WEHI164s fibrosarcoma cell line (provided by the Institute of Development, Aging and Cancer, Tohoku University). Pravastatin was obtained from Daiichi-Sankyo (Tokyo, Japan).

2.3. Neonatal rat cardiomyocyte preparation

Primary ventricular myocytes were isolated from neonatal rats, purified by Percoll density gradient centrifugation, and pre-plated for 1 h to enrich for cardiac myocytes (95%). The obtained cells were plated at a density of 7.5×10^5 cells per well (3.5-cm diameter), and then cultured in Dulbecco's Modified Eagle Medium (Invitrogen, Camarillo, CA, USA) containing 10% fetal calf serum, 2 μM glutamine, and 1% penicillin/streptomycin at 37 °C in a humidified 5% CO_2 incubator [18].

2.4. Monocyte-endothelial cell adhesion assay

We previously reported that LTα_3 increases monocyte-endothelial interactions *in vitro* [12]. To investigate the effects of LTα C804A polymorphism and statin treatment on monocyte-endothelial cell interactions, cell adhesion assays involving THP1 cells and HUVEC were conducted. As LTα C804A polymorphism replaces threonine with asparagine at residue 26 (Thr26Asn) in the LTα_3 protein, recombinant 26Thr- and 26Asn-LTα_3 were compared. For the assay, HUVEC were first cultured in 96-well microplates (Asahi Techno Glass, Tokyo, Japan) for two days to form monolayers, and were then incubated with 1 ng/ml 26Thr-LTα_3 or 26Asn-LTα_3 for 5 h prior to performing the adhesion assay. The effects of pravastatin treatment on adhesion of THP1 cells to HUVEC were also examined by adding 10 μM pravastatin to HUVEC cultures 12 h before stimulation with LTα_3 [12]. Further details of this assay are shown in supplementary method.

2.5. Vascular cell adhesion molecule 1 (VCAM1) assay

To determine the influence of 26Thr-LTα_3 and 26Asn-LTα_3 on the expression of VCAM1, Western blot analysis was performed as previously described [12]. Briefly, total cellular protein (10–20 μg) was obtained from HUVEC after stimulation with 1 ng/ml 26Thr-LTα_3 or 26Asn-LTα_3 for 6 h. To evaluate whether the effects of 26Thr-LTα_3/26Asn-LTα_3 on VCAM1 expression were influenced by pravastatin treatment, 10 μM pravastatin was added 12 h before 26Thr-LTα_3/26Asn-LTα_3 stimulation of HUVEC cultures. VCAM1 and actin were detected using anti-VCAM1 and anti-actin antibodies, respectively (Santa Cruz Biotechnology, Santa Cruz, CA, USA).

2.6. Monocyte migration assay

The migration of monocytes to HUVEC was analyzed using a modified Boyden chamber method. Briefly, HUVEC were cultured in the lower compartments of 24-well Transwell® microplates (Corning, Acton, MA, USA) for two days to form a monolayer. To investigate the effects of LTα C804A polymorphism on the migration of THP1 cells to HUVEC, HUVEC were incubated with 1 ng/ml 26Thr-LTα_3 or 26Asn-LTα_3 for 5 h prior to performing the migration assay. We also examined the effects of pravastatin treatment on monocytes migration by adding 10 μM pravastatin to HUVEC cultures 12 h before stimulation with LTα_3. Further details of this assay are shown in Supplementary Methods.

2.7. Endoplasmic reticulum (ER) stress in rat neonatal cardiomyocytes

ER stress induced by LTα_3 on rat neonatal cardiomyocytes was evaluated by treating rat cardiomyocytes with either 10 ng/ml 26Thr-LTα_3 or 26Asn-LTα_3 for 24 h. The effects of pravastatin on 26Thr-LTα_3/26Asn-LTα_3-induced ER stress were evaluated by adding 10 μM pravastatin to cultures of rat cardiomyocytes 24 h before stimulation with LTα_3. For Western blot analysis, Glucose-regulated

protein 94 kDa (GRP94) and 78 kDa (GRP78) were detected using anti-GRP94 and anti-GRP78 antibodies, respectively (Assay Designs, Ann Arbor, MI, USA), and GAPDH was detected using anti-GAPDH antibody (Millipore, Billerica, MA, USA).

2.8. Statistical analysis

All statistical analyses were performed with either SPSS 11.0 software (SPSS Inc., Tokyo, Japan) or R software (http://www.R-project.org/). For epidemiologic analysis, discrete variables were expressed as counts or percentages, as indicated, and compared with the χ^2-test. Continuous variables were expressed as the mean ± SD and compared using the unpaired Student's *t*-test. Survival curves were constructed using the Kaplan–Meier method and differences in mortality rates were compared between groups with the Log-rank test. Cox regression analyses were used to determine whether LTα C804A polymorphism was an independent predictor of mortality. For experimental analysis, data are presented as the mean ± SE. Statistical significance was determined by the unpaired Student's *t*-test or one-way ANOVA followed by Bonferroni's correction, except for the analysis of GRP78/94, for which Mann–Whitney's *U* test was used. All reported *p* values are two-sided, and statistical significance was defined as $p < 0.05$.

3. Results

3.1. Impact of LTα C804A polymorphism on mortality and statin treatment in post-AMI patients

Among 10,076 consecutive Japanese AMI patients who were registered in the Osaka Acute Coronary Insufficiency Study (OACIS) between 1998 and 2008, typing for this polymorphism was conducted for 3506 post AMI patients, and successful typing was obtained for 3486 patients, which denotes call rate was 99.4% (Suppl. Fig. 1). The prevalence of the C804A genotypes was as follows: CC 1333(38.2%), CA 1592(45.7%), AA 561(16.1%) ($p = 0.020$ by Hardy–Weinberg equilibrium test) (Suppl. Table 1).

After comparing the incidence of all-cause mortality among patients with the three genotypes of LTα C804A polymorphism, a similar trend of increasing mortality for patients with the AA and CA genotypes was detected (Suppl. Fig. 2). Therefore, we selected LTα C804A polymorphism as a dominant parameter and compared the incidence of all-cause mortality between patients with the AA or CA genotype (A allele carriers) and those with the CC genotype (non-A allele carriers). The baseline characteristics of all subjects and the two patient subgroups, consisting of those with (statin(+)) and without (statin(−)) statin treatment at discharge, are shown in Table 1 and Suppl. Table 2. In both patient subgroups, no significant differences were detected in the baseline characteristics between LTα 804A allele carriers (AA + CA genotypes) and non-804A allele carriers (CC genotypes), except for age and reperfusion therapy. Age was significantly younger and reperfusion rate was significantly higher in the former subgroup.

A total of 247 deaths were recorded during the median follow-up period of 1775 days. Kaplan–Meier curves were constructed for patients based on LTα C804A polymorphism (Fig. 1A), revealing that 804A allele carriers had significantly higher all-cause mortality than that of non-804A allele carriers (7.9% vs. 5.7%, $p = 0.011$). We also plotted Kaplan–Meier curves for all-cause mortality among subgroups that were divided based on treatment with statins at discharge (Fig. 1B). For patients not receiving statin therapy (statin(−)), all-cause mortality was significantly higher in 804A carriers compared to non-804A carriers (9.8% vs. 6.8%, $p = 0.025$), but did not differ among those receiving statin therapy (statin(+)) (5.0% vs. 4.2%, $p = 0.345$), suggesting that the mortality effects of LTα C804A polymorphism are influenced by statin therapy.

Table 1
Patient demographics based on lymphotoxin alpha C804A polymorphism.

	LTA 804 polymorphism		*p* Value
	Non-A allele carrier (CC)	A allele carrier (AA + AC)	
	N = 1333	*N* = 2153	
Age (y.o.)	64.7 ± 11.0	63.9 ± 11.4	0.035
Male (%)	77.8	78.1	0.853
BMI (kg/m^2)	23.9 ± 3.4	23.8 ± 3.4	0.686
DM (%)	31.0	34.2	0.053
HT (%)	58.9	59.2	0.869
HL (%)	48.5	47.0	0.404
Smoking (%)	64.6	65.3	0.691
OMI (%)	10.5	11.5	0.343
AP (%)	24.2	24.8	0.695
Admission < 24 h (%)	39.9	38.3	0.335
STEMI (%)	86.4	86.5	0.959
peak CK > 3000 (%)	31.6	34.8	0.061
Killip > 1 at admission (%)	11.8	13.3	0.193
T-Cho (mg/dl) at admission	197.9 ± 42.9	195.6 ± 44.7	0.145
HDL-Cho (mg/dl)	46.8 ± 12.7	46.1 ± 12.3	0.093
Multi-vessel disease (%)	33.9	37.3	0.050
Reperfusion therapy (%)	89.5	91.8	0.023
Stent (%)	78.8	77.0	0.249
Thrombectomy (%)	39.1	39.4	0.883
Final TIMI3 (%)	89.2	88.1	0.338
ACEIs (%)	54.4	54.9	0.768
ARBs (%)	23.9	24.2	0.842
ACEIs or ARBs (%)	76.4	76.6	0.921
Beta blockers (%)	45.0	47.6	0.135
Ca blockers (%)	21.3	21.1	0.904
Statin (%)	41.4	38.9	0.145
Diuretics (%)	24.8	27.7	0.057
Anti-platelets (%)	98.3	98.2	0.800
Nitrates (%)	37.7	39.5	0.304
Anti-coagulants (%)	18.8	18.4	0.816
T-Cho (mg/dl) at discharge	186.9 ± 35.1	185.4 ± 36.4	0.339
HDL-Cho (mg/dl)	38.8 ± 10.7	38.0 ± 10.7	0.110

Patient characteristics between LTα 804A allele carriers (AA + AC) and non-804A allele carriers (CC).
Discrete variables are expressed as counts or percentages, as indicated, and were compared with the χ^2-test. Continuous variables are expressed as the mean ± SD, and were compared with the unpaired Student's *t*-test.
LTα = lymphotoxin alpha; BMI = body mass index; DM = diabetes mellitus; HT = hypertension; HL = hyperlipidemia; OMI = old myocardial infarction; AP = angina pectoris; STEMI = ST elevation myocardial infarction; CK = creatinine kinase; T-Cho = total cholesterol; HDL-Cho = high density lipoprotein cholesterol; PCI = percutaneous coronary intervention; emergent PCI = PCI performed within 24 h after the onset of MI; Multi-vessel disease = two or three vessel disease; Final TIMI3 = final TIMI3 acquisition at reperfusion therapy; ACEI = angiotensin converting enzyme inhibitor; ARB = angiotensin II receptor blocker; Ca blockers = calcium channel antagonists at discharge.

Cox's proportional hazard analysis confirmed that the 804A allele was significantly associated with increased mortality (Table 2, adjusted HR 1.44, 95% CI: 1.06–1.95, $p = 0.018$). Interestingly, this trend was evident for patients without statin treatment at discharge (adjusted HR 1.48, 95% CI: 1.03–2.12, $p = 0.034$), but not for those who were treated with statins at discharge (adjusted HR: 1.22, 95% CI: 0.70–2.10, $p = 0.486$) (Table 2).

3.2. LTα-induced adhesion of THP1 cells to endothelial cells is attenuated by pravastatin

As shown in Fig. 2A, both 26Thr-LTα_3 and 26Asn-LTα_3, corresponding to LTα 804C- and 804A-polymorphic proteins, respectively, increased the adhesion of THP1 cells to HUVEC monolayers when compared with controls ($p < 0.001$). Notably, exposure of HUVEC to 26Asn-LTα_3 led to greater increases in the adhesion rate

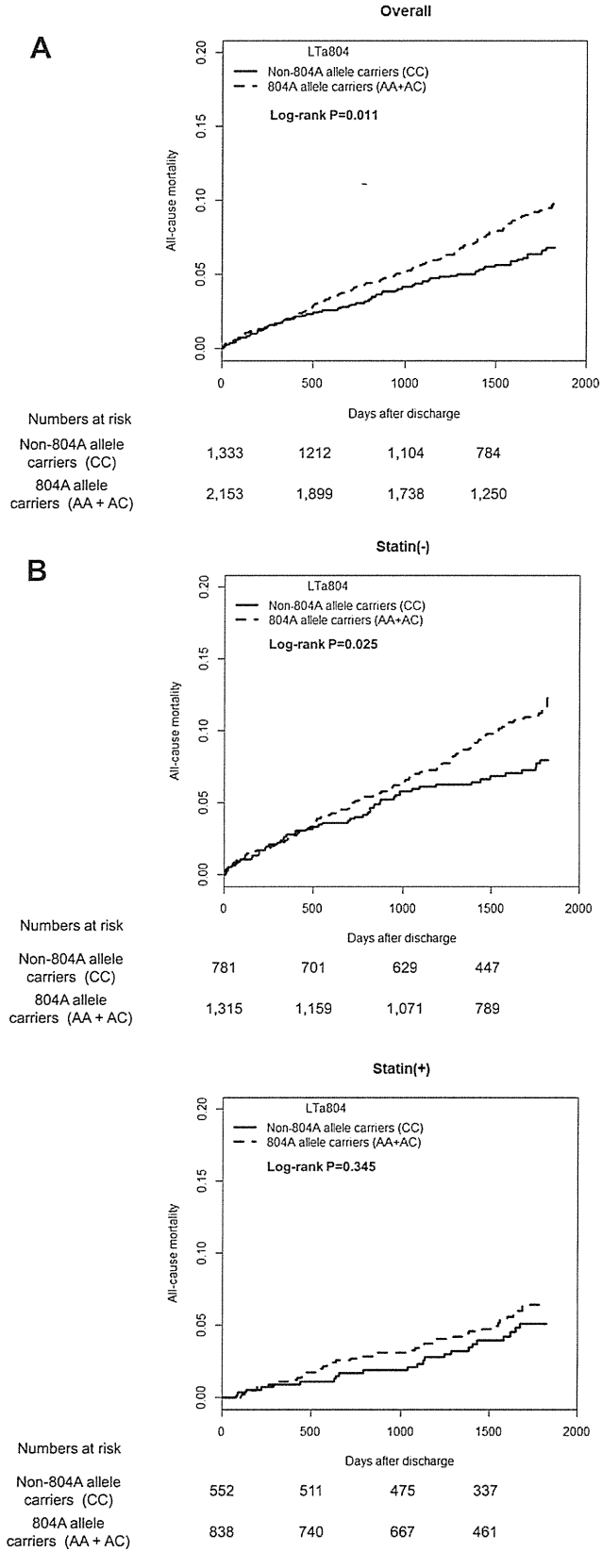

Fig. 1. All-cause mortality for AMI patients in relation to LTα C804A polymorphism and statin treatment. A. All-cause mortality rate was significantly higher in LTα 804A allele carriers (AA + AC, $N = 2153$) (dotted line) than in non-804A allele carriers (CC, $N = 1333$) (solid line) ($p = 0.011$ by the Log-rank test). B. All-cause mortality rate was significantly higher in LTα 804A allele carriers (AA + AC) (dotted line) than in non-804A allele carriers (CC) (solid line) in the subgroup without statin therapy (statin(−)) ($p = 0.025$ by the Log-rank test), whereas no difference was detected between the LTα C804A polymorphism groups for those that received statin therapy (statin(+)) ($p = 0.345$ by the Log-rank test).

Table 2
Hazard ratio for all-cause mortality among LTα 804A allele carriers in the presence or absence of statin prescription at discharge.

	Death	Total *N*	HR	95% CI	*p* Value
Model 1					
Overall	247	3486	1.42	1.08–1.86	0.011
Statin(−)	182	2096	1.44	1.04–1.98	0.026
Statin(+)	65	1390	1.28	0.77–2.12	0.346
Model 2					
Overall	247	3486	1.49	1.14–1.96	0.004
Statin(−)	182	2096	1.54	1.12–2.13	0.008
Statin(+)	65	1390	1.33	0.80–2.20	0.278
Model 3					
Overall	199	3024	1.40	1.04–1.89	0.027
Statin(−)	144	1784	1.48	1.03–2.12	0.034
Statin(+)	55	1240	1.22	0.70–2.10	0.486

Model 1. Hazard ratio of LTα 804A allele carriers (AA + AC) for all-cause mortality (unadjusted).
Model 2. The hazard ratio of LTα 804A-allele carriers on all-cause mortality after being discharged alive was analyzed by Cox regression analysis. Covariates were age and sex.
Model 3. Model 2 + diabetes mellitus, hypertension, hyperlipidemia, smoking history, peak CK ≥ 3,000, multi-vessel disease, reperfusion therapy, and ACEI/ARBs, beta blockers at discharge.
Abbreviations are the same as those used in Table 1.

compared to that of 26Thr-LTα_3 (2.36 vs. 2.03 fold, respectively, compared with control; $p < 0.05$), although the rate decreased and was comparable between the groups (1.58 vs. 1.43 fold, respectively, p = n.s.) after the pretreatment of HUVEC with pravastatin. Western blotting revealed that the expression level of VCAM1 on HUVEC was markedly increased by treatment with 26Asn-LTα_3 compared to that with 26Thr-LTα_3. However, both 26Asn- and 26Thr-LTα_3-induced VCAM1 expression was attenuated at similar levels by pravastatin (Fig. 2B).

3.3. LTα-induced monocyte migration is attenuated by pravastatin

In a two-chamber migration assay, the migration rate of THP1 towards the HUVEC-conditioned medium markedly increased by exposure to 26Thr-LTα_3 and 26Asn-LTα_3 when compared with controls ($p < 0.001$). In the absence of pravastatin pretreatment, the migration ratio displayed a larger increase for 26Asn-LTα_3 stimulation compared to 26Thr-LTα_3 (2.14 vs. 1.55 fold compared with control, $p < 0.05$), whereas the two LTα proteins displayed similar small effects in the presence of pravastatin (1.48 vs. 1.46 fold compared with control, p = n.s.) (Fig. 2C).

3.4. LTα-induced ER stress in rat cardiomyocytes is attenuated by pravastatin

GRP78 expression levels in rat neonatal cardiomyocytes were increased by LTα_3 stimulation after 24 h when compared with controls ($p < 0.001$) (Fig. 3A and B). Exposure to 26Asn-LTα_3 led to greater GRP78 expression compared to that induced by 26Thr-LTα_3 (1.68 vs. 1.53 fold compared with control, $p < 0.05$ by Mann–Whitney's U test), although no differences in expression were detected after the pretreatment of cardiomyocytes with 10 μM pravastatin (p = n.s.). Similarly, GRP94 expression was also markedly increased following 26Asn-LTα_3 stimulation compared to exposure to 26Thr-LTα_3 (1.83 vs. 1.59 fold compared with control, $p < 0.05$ by Mann–Whitney's U test) (Fig. 3C and D), and no

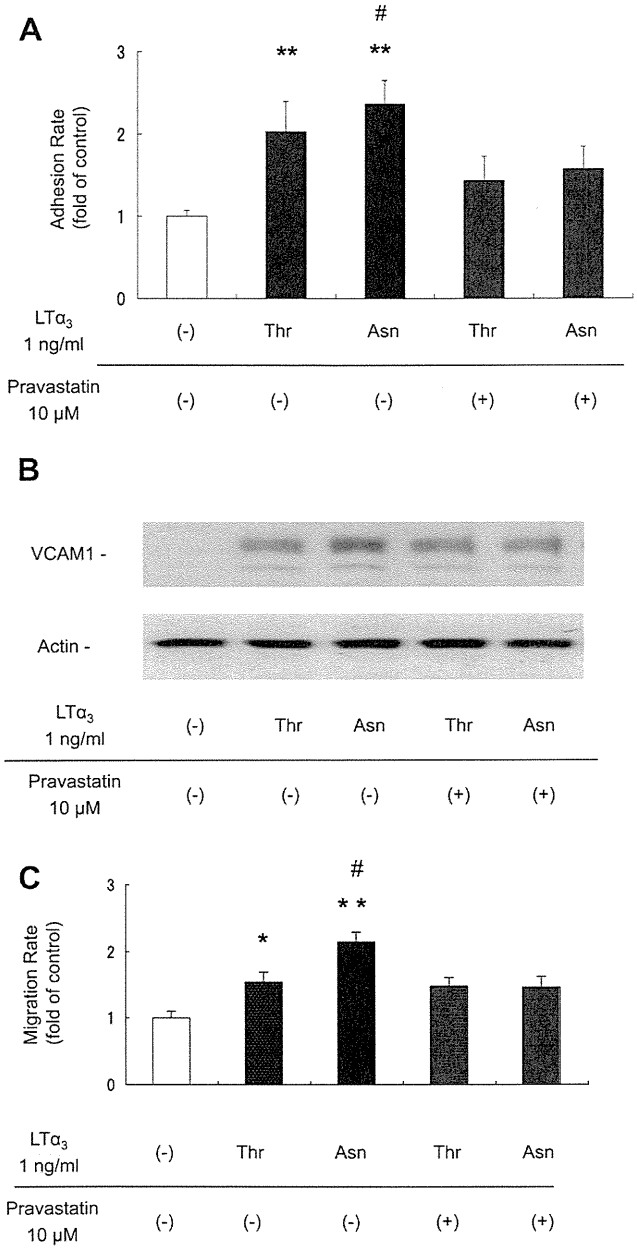

Fig. 2. Effects of LTα C804A polymorphism on monocyte-endothelial adhesion (A) and induction of VCAM1 expression (B) in the absence and presence of pravastatin treatment. Effect of LTα C804A polymorphism on THP1 cell migration rate (C). A. The adhesion rate of THP1 onto HUVEC was increased by both 26Thr-LTα$_3$ and 26Asn-LTα$_3$ stimulation of HUVEC. The adhesion rate was higher when cells were stimulated by 26Asn-LTα$_3$ than by 26Thr-LTα$_3$ (**$p < 0.001$ vs. control, #$p < 0.05$ vs. 26Thr-LTα$_3$ protein by the unpaired t-test), but the difference was reduced by the pretreatment of cells with 10 μM pravastatin. B. The expression levels of VCAM1 were increased by 26Thr-LTα$_3$ or 26Asn-LTα$_3$ stimulation in comparison with control. 26Asn-LTα$_3$ led to greater induction of VCAM1 expression compared to 26Thr-LTα$_3$, but VCAM1 was expressed at comparable levels for both proteins following the pretreatment of HUVEC with 10 μM pravastatin. A representative result among five independent experiments is shown. C. The migration rate of THP1 towards HUVEC was increased by both 26Thr-LTα$_3$ and 26Asn-LTα$_3$, although the rate was higher for cells stimulated with 26Asn-LTα$_3$ (2.14 vs. 1.55 fold when compared with control, **$p < 0.001$ vs. control, *$p < 0.01$ vs. control, and #$p < 0.05$ vs. 26Thr-LTα$_3$ by the unpaired t-test). However, no significant differences were detected between the two proteins following the pretreatment of HUVEC with 10 μM pravastatin (1.48 vs. 1.46 fold when compared with control by the unpaired t-test).

differences in expression were detected after pravastatin pretreatment (p = n.s.).

4. Discussion

We previously reported the clinical impacts of polymorphisms in the genes encoding LTα and its related proteins on susceptibility to AMI and increased post-AMI mortality. The results of the present study further underline the importance of the LTα cascade in the pathogenesis of cardiovascular diseases by showing that a functional SNP in the LTα gene at C804A, which replaces threonine with asparagine at residue 26 (Thr26Asn), is associated with increased all-cause mortality after AMI. Furthermore, our findings suggest that LTα gene polymorphism has clinical significance as a therapeutic target, because a reduction of 26Asn-associated mortality risk by statin treatment was suggested in the cohort of post-AMI patients, as well as in the *in-vitro* experimental studies.

We found that LTα C804A polymorphism is also associated with increased mortality among AMI patients registered in OACIS, a prospective observational study of AMI being conducted in Osaka, Japan. However, this result was not entirely unexpected, as we previously reported that A252G polymorphism in the LTα gene, which has a strong linkage disequilibrium with C804A, is associated with increased post-AMI mortality [14]. Therefore, the most important finding of the present study was the demonstration of the pharmacological modification of the C804A-related mortality risk with statin treatment in the secondary prevention setting of post-AMI. Our findings also suggest that the pharmacological modification mediated by statin might be attributable to decreased monocyte-endothelial interaction and ER stress in cardiomyocytes.

The growth of atherosclerotic lesions involves the inflammatory response and is characterized by the adhesion of monocytes onto endothelial cells, migration of monocytes into intima, scavenging of lipoprotein particles, followed by the formation of foam cells and secretion of various pro-inflammatory cytokines [19]. We recently demonstrated that LTα$_3$ stimulation induces the expression of various genes involved in inflammation and cell adhesion, including VCAM1, which is a key player in the binding of monocytes to endothelial cells [20], in HUVEC and human coronary arterial endothelial cells [12,21]. In the present study, the stimulation of HUVEC with LTα 804A polymorphic protein (26Asn-LTα$_3$) markedly increased both the adhesion and the migration of monocytes to endothelial cells in comparison with LTα 804C polymorphic protein (26Thr-LTα$_3$). Notably, the differences between 26Asn- and 26Thr-LTα$_3$ were attenuated by the pretreatment of cells with pravastatin, a result that is consistent with our epidemiologic data. Additionally, we performed the experiments to elucidate whether or not LTα$_3$ could alter the transformation of monocytes into macrophages by the observation of morphological change with microscopy and by using fluorescent-labeled oxidized low-density lipoprotein (DiI-Ox-LDL, Biomedical Technologies Inc. Stoughton, MA, USA) followed by fluorescence activated cell sorting (FACS). However, we observed no transformation of monocytes into macrophages after LTα$_3$ stimulus, whereas Phorbol 12-myristate 13-acetate (PMA) stimulus induced the transformation.

Several reports have described the role of LTα in inflammation and atherosclerosis. Although the LTα signaling pathway is considered to be similar in part to that of TNFα, LTα appears to play a dominant role in the regulation of atherosclerotic lesion growth. Schreyer et al. [13] showed that TNFα deficiency did not alter lesion development in mice fed an atherogenic diet, whereas the loss of LTα resulted in a three-fold decrease in the amount of lesions. In addition, we previously revealed that LTα is expressed in the atherosclerotic plaques of patients with coronary artery disease [8]. The present data suggest that the increased risk of mortality

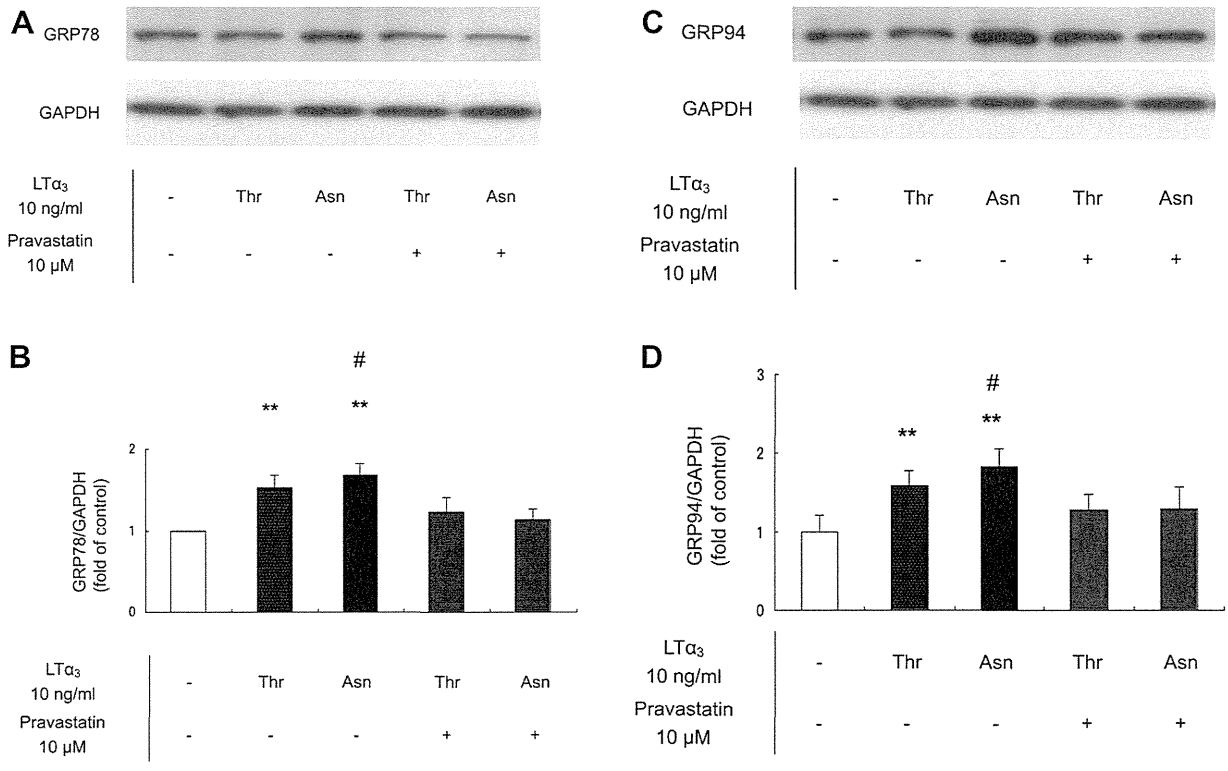

Fig. 3. Effect of LTα C804A polymorphism on the induction of ER stress in rat neonatal cardiomyocytes. The expression levels of glucose-regulated protein (GRP) 78 were increased in rat cardiomyocytes by stimulation with either 26Thr-LTα$_3$ or 26Asn-LTα$_3$ when compared with control cells (**$p < 0.001$) (A and B). 26Asn-LTα$_3$ had a greater effect on GRP78 expression compared to 26Thr-LTα$_3$ (1.68 vs. 1.53 fold when compared with control, #$p < 0.05$), but GRP78 expression induction was attenuated by 10 μM pravastatin pretreatment for both 26Thr-LTα$_3$ and 26Asn-LTα$_3$ (p = n.s.). The expression levels of GRP94 were also increased by 26Thr-LTα$_3$ or 26Asn-LTα$_3$ stimulation when compared with control cells (**$p < 0.001$) (C and D), but were higher for 26Asn-LTα$_3$ compared to 26Thr-LTα$_3$ (1.83 vs. 1.59 fold, #$p < 0.05$). The induction of GRP94 expression was also attenuated by the pretreatment of cardiomyocytes with pravastatin (p = n.s.).

associated with LTα C804A polymorphism can be lowered by statin treatment, and that the beneficial effects of statins for 804A allele carriers might be attributable to the attenuation of monocyte-endothelial interactions and cardiomyocyte degeneration. Previous experimental studies have revealed that statins attenuate the inflammatory response, including the decreased expression of adhesion molecules triggered by TNFα via the NFκB signaling pathway [22–25]. Considering that LTα shares major receptors (TNF receptors type I and II) with TNFα [11], it is reasonable to speculate that statins attenuate the LTα-induced inflammatory response, thereby preventing atherogenesis and cardiovascular events. Our present experimental data support this idea, as 26Asn-LTα$_3$ stimulation led to greater human monocyte-endothelial adhesion and monocyte migration compared to 26Thr-LTα$_3$, and the effects induced by both 26Asn- and 26Thr-LTα$_3$ were blunted and became comparable following pravastatin treatment.

Inflammation induced by pro-inflammatory cytokines is one of the major causes of ER stress, which is characterized by the accumulation of unfolded proteins induced by stimuli such as oxidative stress and ischemia. As ER stress in cardiomyocytes is followed by cardiac remodeling and heart failure [18,26,27], we evaluated whether LTα polymorphism is associated with the occurrence of ER stress. ER stress triggers the unfolded protein response, which involves a group of signal transduction pathways that ameliorate the accumulation of unfolded proteins in the ER by increasing the expression of ER-resident chaperones, such as GRP78/94. Thus, enhanced expression of GRP78/94 can be used as a marker of ER stress. Here, we found that ER stress in rat cardiomyocytes was significantly elevated by 26Asn-LTα$_3$ stimulation compared with that by 26Thr-LTα$_3$, and that these differences were blunted by pravastatin treatment. These findings may partly explain our observation that LTα 804A allele carriers had higher mortality after MI in the absence of statin treatment.

The preventive effects of statin therapy on cardiovascular events have been demonstrated in many clinical studies and are thought to be mediated, at least in part, by the pleiotropic effects, including anti-inflammatory and lipid-lowering activities [28–30]. However, despite considerable research efforts, the pleiotropic effects of statins remain poorly characterized and have yet to be demonstrated in the clinical setting [15]. In the present study, no significant differences were detected in the average total and HDL-cholesterol level between 804A allele and non-804A allele carriers in both statin(+) and statin(−) subgroups, suggesting that LTα polymorphism does not modify cardiovascular risk by altering serum cholesterol levels. Therefore, we speculate that statins may mask the adverse effects of LTα polymorphisms via their pleiotropic properties, independently of their lipid-lowering effects.

Several limitations of our study warrant mention. First, the epidemiologic analyses were based on an observational study, and statin prescriptions were not randomized. However, the bias was likely minimal, because statins were prescribed by attending physicians without knowledge of patients' LTα genotype, and as a consequence, statin prescription was naturally "genetically randomized". Second, data on the daily doses, adherence, and discontinuation of statin treatment after discharge were lacking, despite the possibility that these factors may have modified the actual impact of statin therapy on LTα polymorphism. Third, although we found that LTα polymorphism is associated with mortality after the onset of AMI in our patient cohort comprised of Asian people who were predominantly Japanese, further analysis is

needed to verify the results in other ethnic groups. Fourth, the study included only the patients with informed consent, who were in relatively less severity after the onset of MI, which is also a study limitation.

In conclusion, our results demonstrate that the LTα 804A allele is significantly associated with increased mortality in post-AMI patients, a finding that may be attributable to the increased mortality risk of the 804A allele in the absence of statin treatment. Therefore, post-AMI patients with LTα C804A polymorphism may be good candidates for pharmacological intervention with statins to improve long-term mortality. Although further investigations are needed, genetic polymorphisms of LTα, including C804A, may represent suitable therapeutic targets in the near future.

Funding

This work was supported in part by Grants-in-Aid for scientific research from the Ministry of Education, Culture, Sports, Science, and Technology, Japan to Y. Sakata (#19590816) and H. Sato (#19390215).

Conflict of interest

None of the authors have conflicts of interest to declare.

Appendix A. Supplementary data

Supplementary data related to this article can be found at http://dx.doi.org/10.1016/j.atherosclerosis.2013.01.020.

References

[1] Jernberg T, Johanson P, Held C, Svennblad B, Lindback J, Wallentin L. Association between adoption of evidence-based treatment and survival for patients with ST-elevation myocardial infarction. J Am Med Assoc 2011;305:1677–84.
[2] Fox KA, Steg PG, Eagle KA, et al. Decline in rates of death and heart failure in acute coronary syndromes, 1999–2006. J Am Med Assoc 2007;297:1892–900.
[3] Ozaki K, Sato H, Inoue K, et al. SNPs in BRAP associated with risk of myocardial infarction in Asian populations. Nat Genet 2009;41:329–33.
[4] Ozaki K, Sato H, Iida A, et al. A functional SNP in PSMA6 confers risk of myocardial infarction in the Japanese population. Nat Genet 2006;38:921–5.
[5] The PROCARDIS Consortium. A trio family study showing association of the lymphotoxin-alpha N26 (804A) allele with coronary artery disease. Eur J Hum Genet 2004;12:770–4.
[6] Ozaki K, Inoue K, Sato H, et al. Functional variation in LGALS2 confers risk of myocardial infarction and regulates lymphotoxin-alpha secretion in vitro. Nature 2004;429:72–5.
[7] Iwanaga Y, Ono K, Takagi S, et al. Association analysis between polymorphisms of the lymphotoxin-alpha gene and myocardial infarction in a Japanese population. Atherosclerosis 2004;172:197–8.
[8] Ozaki K, Ohnishi Y, Iida A, et al. Functional SNPs in the lymphotoxin-alpha gene that are associated with susceptibility to myocardial infarction. Nat Genet 2002;32:650–4.
[9] Gray PW, Aggarwal BB, Benton CV, et al. Cloning and expression of cDNA for human lymphotoxin, a lymphokine with tumour necrosis activity. Nature 1984;312:721–4.
[10] Granger GA, Williams TW. Lymphocyte cytotoxicity in vitro: activation and release of a cytotoxic factor. Nature 1968;218:1253–4.
[11] Ruddle NH, Waksman BH. Cytotoxic effect of lymphocyte-antigen interaction in delayed hypersensitivity. Science 1967;157:1060–2.
[12] Suna S, Sakata Y, Shimizu M, et al. Lymphotoxin-alpha3 mediates monocyte-endothelial interaction by TNFR I/NF-kappaB signaling. Biochem Biophys Res Commun 2009;379:374–8.
[13] Schreyer SA, Vick CM, LeBoeuf RC. Loss of lymphotoxin-alpha but not tumor necrosis factor-alpha reduces atherosclerosis in mice. J Biol Chem 2002;277:12364–8.
[14] Mizuno H, Sato H, Sakata Y, et al. Impact of atherosclerosis-related gene polymorphisms on mortality and recurrent events after myocardial infarction. Atherosclerosis 2006;185:400–5.
[15] Barber MJ, Mangravite LM, Hyde CL, et al. Genome-wide association of lipid-lowering response to statins in combined study populations. PLoS One 2010;5:e9763.
[16] Kurotobi T, Sato H, Kinjo K, et al. Reduced collateral circulation to the infarct-related artery in elderly patients with acute myocardial infarction. J Am Coll Cardiol 2004;44:28–34.
[17] Yamada Y, Miyauchi A, Takagi Y, Tanaka M, Mizuno M, Harada A. Association of the C-509–>T polymorphism, alone of in combination with the T869–>C polymorphism, of the transforming growth factor-beta1 gene with bone mineral density and genetic susceptibility to osteoporosis in Japanese women. J Mol Med 2001;79:149–56.
[18] Zhao H, Liao Y, Minamino T, et al. Inhibition of cardiac remodeling by pravastatin is associated with amelioration of endoplasmic reticulum stress. Hypertens Res 2008;31:1977–87.
[19] Libby P. Inflammation in atherosclerosis. Nature 2002;420:868–74.
[20] Galkina E, Ley K. Vascular adhesion molecules in atherosclerosis. Arterioscler Thromb Vasc Biol 2007;27:2292–301.
[21] Suna S, Sakata Y, Sato H, et al. Up-regulation of cell adhesion molecule genes in human endothelial cells stimulated by lymphotoxin alpha: DNA microarray analysis. J Atheroscler Thromb 2008;15:160–5.
[22] Wang HR, Li JJ, Huang CX, Jiang H. Fluvastatin inhibits the expression of tumor necrosis factor-alpha and activation of nuclear factor-kappaB in human endothelial cells stimulated by C-reactive protein. Clin Chim Acta 2005;353:53–60.
[23] Planavila A, Laguna JC, Vazquez-Carrera M. Atorvastatin improves peroxisome proliferator-activated receptor signaling in cardiac hypertrophy by preventing nuclear factor-kappa B activation. Biochim Biophys Acta 2005;1687:76–83.
[24] Inoue I, Itoh F, Aoyagi S, et al. Fibrate and statin synergistically increase the transcriptional activities of PPARalpha/RXRalpha and decrease the transactivation of NFkappaB. Biochem Biophys Res Commun 2002;290:131–9.
[25] Rasmussen LM, Hansen PR, Nabipour MT, Olesen P, Kristiansen MT, Ledet T. Diverse effects of inhibition of 3-hydroxy-3-methylglutaryl-CoA reductase on the expression of VCAM-1 and E-selectin in endothelial cells. Biochem J 2001;360:363–70.
[26] Minamino T, Komuro I, Kitakaze M. Endoplasmic reticulum stress as a therapeutic target in cardiovascular disease. Circ Res 2010;107:1071–82.
[27] Okada K, Minamino T, Tsukamoto Y, et al. Prolonged endoplasmic reticulum stress in hypertrophic and failing heart after aortic constriction: possible contribution of endoplasmic reticulum stress to cardiac myocyte apoptosis. Circulation 2004;110:705–12.
[28] Ridker PM, Cannon CP, Morrow D, et al. C-reactive protein levels and outcomes after statin therapy. N Engl J Med 2005;352:20–8.
[29] Wilt TJ, Bloomfield HE, MacDonald R, et al. Effectiveness of statin therapy in adults with coronary heart disease. Arch Intern Med 2004;164:1427–36.
[30] Bonetti PO, Lerman LO, Napoli C, Lerman A. Statin effects beyond lipid lowering–are they clinically relevant? Eur Heart J 2003;24:225–48.

Cardiovasc Drugs Ther (2013) 27:125–132
DOI 10.1007/s10557-012-6437-6

ORIGINAL ARTICLE

Liposomal Amiodarone Augments Anti-arrhythmic Effects and Reduces Hemodynamic Adverse Effects in an Ischemia/Reperfusion Rat Model

Hiroyuki Takahama · Hirokazu Shigematsu · Tomohiro Asai · Takashi Matsuzaki · Shoji Sanada · Hai Ying Fu · Keiji Okuda · Masaki Yamato · Hiroshi Asanuma · Yoshihiro Asano · Masanori Asakura · Naoto Oku · Issei Komuro · Masafumi Kitakaze · Tetsuo Minamino

Published online: 24 January 2013

Abstract
Purpose Although amiodarone is recognized as the most effective anti-arrhythmic drug available, it has negative hemodynamic effects. Nano-sized liposomes can accumulate in and selectively deliver drugs to ischemic/reperfused (I/R) myocardium, which may augment drug effects and reduce side effects. We investigated the effects of liposomal amiodarone on lethal arrhythmias and hemodynamic parameters in an ischemia/reperfusion rat model.
Methods and Results We prepared liposomal amiodarone (mean diameter: 113±8 nm) by a thin-film method. The left coronary artery of experimental rats was occluded for 5 min followed by reperfusion. Ex vivo fluorescent imaging revealed that intravenously administered fluorescent-labeled nano-sized beads accumulated in the I/R myocardium. Amiodarone was measurable in samples from the I/R myocardium when liposomal amiodarone, but not amiodarone, was administered. Although the intravenous administration of amiodarone (3 mg/kg) or liposomal amiodarone (3 mg/kg) reduced heart rate and systolic blood pressure compared with saline, the decrease in heart rate or systolic blood pressure caused by liposomal amiodarone was smaller compared with a corresponding dose of free amiodarone. The intravenous administration of liposomal amiodarone (3 mg/kg), but not free amiodarone (3 mg/kg), 5 min before ischemia showed a significantly reduced duration of lethal arrhythmias (18±9 s) and mortality (0 %) during the reperfusion period compared with saline (195±42 s, 71 %, respectively).
Conclusions Targeting the delivery of liposomal amiodarone to ischemic/reperfused myocardium reduces the mortality due to lethal arrhythmia and the negative hemodynamic changes caused by amiodarone. Nano-size liposomes may be a promising drug delivery system for targeting I/R myocardium with cardioprotective agents.

Keywords Liposome · Amiodarone · Lethal arrhythmia · Ischemia · Reperfusion

T. Matsuzaki · S. Sanada · H. Y. Fu · K. Okuda · M. Yamato · Y. Asano · I. Komuro · T. Minamino (✉)
Department of Cardiovascular Medicine, Osaka University Graduate School of Medicine, 2-2 Yamadaoka, Suita, Osaka 565-0871, Japan
e-mail: minamino@cardiology.med.osaka-u.ac.jp

H. Takahama · M. Asakura · M. Kitakaze
Department of Cardiovascular Medicine, National Cerebral and Cardiovascular Center, Suita 565-8565, Japan

H. Shigematsu · T. Asai · N. Oku
Department of Medical Biochemistry and Global COE, University of Shizuoka Graduate School of Pharmaceutical Sciences, Shizuoka 422-8526 Shizuoka, Japan

H. Asanuma
Department of Cardiovascular Science and Technology, Kyoto Prefectural University School of Medicine, Kyoto 602-8566, Japan

H. Takahama
Division of Cardiovascular Disease, Mayo Clinic, Rochester, MN 55902, USA

Introduction

Therapies for the prevention and treatment of ischemia-induced life-threatening arrhythmias remain an unmet medical need [1]. Amiodarone is currently considered to be the most effective anti-arrhythmic drug available for treating life-threatening arrhythmias [2, 3], despite the fact that this compound has a negative impact on hemodynamic parameters [4, 5]. The intravenous administration of amiodarone is expected

to be beneficial for the immediate treatment of arrhythmias in emergency settings, such as acute myocardial infarction (AMI) [6, 7]. However, in clinical practice, the administration of amiodarone remains problematic for the treatment of AMI [8]. Although lower doses of amiodarone result in fewer incidences of death, high doses of amiodarone can cause hypotension and non-cardiac death, both of which may diminish the positive effects of amiodarone [8, 9]. Therefore, a novel delivery system is strongly desired to enhance the anti-arrhythmic effects of amiodarone without producing severe side effects.

Liposomes are widely used for drug delivery to actively or passively target specific organs and to improve drug stability in cancer and inflammatory diseases [10–12]. In ischemic/reperfused (I/R) myocardium, cellular permeability is enhanced and vascular endothelial integrity is disrupted [13, 14], suggesting that nanoparticles, such as liposomes, may be a promising drug delivery system for targeting I/R myocardium with cardioprotective agents [15]. Indeed, we have recently demonstrated that adenosine encapsulated by liposomes coated with polyethylene glycol (PEG) exhibited enhanced cardioprotective effects and attenuated side effects, such as hypotension and bradycardia, in an ischemia/reperfusion model of rats [16]. In the present study, we prepared liposomal amiodarone and examined 1) the targeted accumulation of liposomal amiodarone in the I/R myocardium, 2) the hemodynamic effects of the intravenous administration of liposomal amiodarone and free amiodarone, and 3) the anti-arrhythmic effects of these preparations in an I/R rat model. We showed that targeting the delivery of liposomal amiodarone to I/R myocardium reduces the mortality due to lethal arrhythmias and the negative hemodynamic changes caused by amiodarone in an I/R rat model.

Methods

Materials

The materials used to prepare PEGylated liposomes, including 1-palmitoyl-2-oleoyl-sn-glycero-3-phosphocholine (POPC), 1,2-dipalmitoyl-sn-glycero-3-phosphocholine (DPPC), cholesterol, and 1,2-distearoyl-sn-glycero-3-phosphoethanolamine-N-poly(ethylene glycol) 2000 (DSPE-PEG2000), were kindly donated by Nippon Fine Chemical Co. (Takasago, Hyogo, Japan). Fluorescent beads (diameter 100 nm) were purchased from Invitrogen. All other materials were obtained from Sigma-Aldrich (St. Louis, MO, USA).

Animals

Male Wistar rats (9 weeks old and weighing 250–310 g; Japan Animals, Osaka, Japan) were used. The animal experiments were approved by the Osaka University Research Committee and were performed according to institutional guidelines. All studies conformed to the Guide for the care and Use of Laboratory Animals published by the US National Institutes of Health (NIH Publication No. 85–23, revised 1996).

Preparation of PEGylated Liposomes

PEGylated liposomes composed of POPC, DPPC, cholesterol, DSPE-PEG2000, and amiodarone were prepared by a thin-film method. Briefly, amiodarone and lipids dissolved in chloroform were evaporated to form a thin lipid film using a rotary evaporator. The lipid film was dried for at least 1 h under reduced pressure and then hydrated with PBS (pH7.4). The liposome solution was freeze-thawed for 3 cycles with liquid nitrogen. The particle size of the liposomes was adjusted by extrusion through 100-nm-pore polycarbonate filters (Nuclepore, Cambridge, MA, USA). The liposomal solutions were centrifuged at 453,000 g for 15 min (CS120GXL, Hitachi, Japan) to remove the untrapped amiodarone. Then, the liposomes were resuspended in PBS. To determine the efficacy of trapping amiodarone in the liposomes, an aliquot of the liposomal solution was solubilized with 1 % reduced Triton X-100 (Sigma-Aldrich), and the amount of amiodarone was optically determined at 240 nm.

Characterization of PEGylated Liposomes

The particle size and ζ potential of PEGylated liposomes diluted with PBS were measured by dynamic scatter analysis (Zetasizer Nano ZS; Malvern, Worcestershire, UK). The analyses were performed 15 times per sample, and the results represent the analysis of 3 independent experiments.

Experimental Protocol

Targeted Delivery of Fluorescent-labeled Nano-sized Beads to the I/R Myocardium

The rats were anesthetized with intraperitoneal sodium pentobarbital (50 mg/kg). Catheters were advanced into the femoral vein to infuse the drugs. Ischemia/reperfusion was induced by 5 min of left coronary artery occlusion followed by reperfusion [16]. After the hemodynamic parameters became stable, fluorescent-labeled nano-size beads, 100 nm in diameter (FluoSpheres, Invitrogen), were intravenously infused to the rats for 5 min before ischemia or before a sham operation (n=3, each). Fifteen minutes after reperfusion, the hearts were removed and cut into 5 sections parallel to the axis from the base to the apex. Then, ex vivo fluorescence images were obtained with an Olympus SZX12 stereoscopic microscope equipped with a DP71 digital camera (Olympus, Tokyo, Japan) before and after the hearts were sliced.

Targeted Delivery of Amiodarone and Liposomal Amiodarone to the I/R Myocardium

Catheters were advanced into the femoral artery and vein to measure the systemic blood pressure (BP) and to infuse the drugs into the anesthetized rats, respectively. Electrocardiographic and hemodynamic parameters, such as heart rate (HR) and BP, were continuously monitored during the study using a PowerLab system (ADInstruments, Castle Hill, Australia). After the hemodynamic parameters became stable, to clarify the targeted delivery of amiodarone and liposomal amiodarone to the I/R myocardium, we intravenously administered saline, free amiodarone (3 mg/kg) or liposomal amiodarone (3 mg/kg) to rats for 5 min before the onset of ischemia. Then, we obtained blood samples and myocardium from the I/R area.

Effects of Amiodarone and Liposomal Amiodarone on Lethal Arrhythmias

To evaluate the effects of amiodarone and liposomal amiodarone on lethal arrhythmias, we intravenously administered saline (n=7), free amiodarone (3.0 or 10.0 mg/kg) (n=6 each), PEGylated liposomes (empty liposomes) (n=6), and PEGylated liposomal amiodarone (3.0 mg/kg) (n=6) for 5 min before ischemia. The dose of amiodarone used in this study was lower than that used in a previous study [17] to clarify whether amiodarone encapsulated by liposomes coated with PEG exhibited enhanced anti-arrhythmic effects. Without any procedure such as electrical conversion or cardiac massage, ventricular tachyarrhythmias (VT/VF) occurred frequently during early period of reperfusion and the mortality of rats reached more than a half of cases in this model [18].

Measurement of Amiodarone Concentration

The concentration of amiodarone in serum and heart tissue from the I/R area was assayed by high-performance liquid chromatography (HPLC) as previously described [19]. The detection limit of the HPLC assay was 50 ng/mL. Blood and myocardial samples were obtained at the end of the experimental protocol. The sample preparation was performed as previously described [19]. Briefly, myocardium was freed from visible blood, thereafter rinsed with 0.9 % sodium chloride and stored at −20 °C until analysis. After that, myocardial tissue samples were finely minced and 100 mg were homogenized with 0.9 % sodium chloride (1 mL) and after centrifugation, the clear supernatant was injected into HPLC.

Quantitative Evaluation of Fluorescent-labeled Nano-sized Beads in the I/R Myocardium

To analyze the quantitative fluorescent intensity, signals from heart slices were quantified by image analysis (Image J; National Institutes of Health, USA) as previously described [20]. The signal intensity from the heart slices was evaluated as the average signals of the whole heart and the left ventricle (LV) (Fig. 2c).

Arrhythmia Analysis

The electrocardiographic tracings were independently analyzed by two of the authors, who were blinded to the treatment assignment. The duration of each spontaneous ventricular tachycardia or fibrillation episode during the I/R protocol was measured using the time scale provided by the recording software. Ventricular tachycardia was defined as 4 or more consecutive ventricular ectopic beats, and ventricular fibrillation was defined as a signal in which the individual QRS deflections could not easily be distinguished from one another. However, distinguishing ventricular tachycardia from fibrillation was often difficult [21]; therefore, we report ventricular tachycardia and fibrillation collectively as ventricular tachyarrhythmias (VT/VF) in this study. VT/VF duration and mortality were evaluated for 5 min of ischemia followed by 15 min of reperfusion.

Statistical Analysis

The parameters of the liposomes are expressed as the mean ± standard deviation (SD). Other data are expressed as the average ± standard error of the mean (SEM). To compare the parameters of the liposomes, unpaired t-tests were performed. We performed the Welch t-test to compare the amiodarone concentration in the plasma and myocardium. For hemodynamic parameters, the data were assessed with the paired t-test for comparisons to the baseline within a group. One-way repeated-measurement ANOVA followed by post-hoc Bonferroni's multiple comparisons were used for comparisons between groups. To address the differences in VT/VF duration among the groups, we performed a non-parametric (Kruskal-Wallis) test followed by evaluation with the Mann–Whitney U test. The mortality rates were compared using the Fisher's exact probability test. In all analyses, $P<0.05$ was considered to be statistically significant.

Results

Characterization of PEGylated Liposomes

We prepared 5 types of PEGylated liposomes composed of POPC, DPPC, cholesterol, and amiodarone. The ratio of unsaturated lipids (POPC) to saturated lipids (DPPC) varied (Fig. 1). During preparation of the liposomes, the POPC: DPPC:cholesterol:amiodarone molar ratio of 10:0:5:1 exhibited the best encapsulation efficiency for amiodarone compared with the other conditions (Fig. 1).

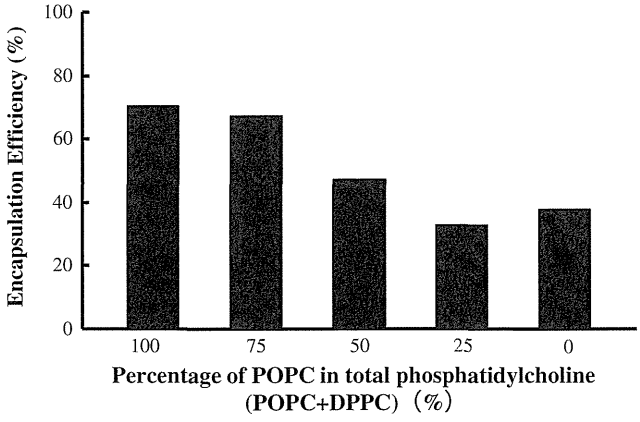

Fig. 1 Encapsulation efficiency of amiodarone in the liposomes. Amiodarone was loaded into liposomes containing POPC, DPPC, or a mixture of POPC and DPPC. The liposomal amiodarone was composed of phosphatidylcholine (POPC + DPPC):cholesterol:amiodarone at a 10:5:1 molar ratio. The percent molar ratio of POPC in total phosphatidylcholine (POPC + DPPC) is indicated in the figure. The encapsulation efficiency of amiodarone was determined as described in the Methods section

The dynamic light scatter analysis showed no significant differences between the mean diameter, polydispersity index, or ζ potential distribution of the empty and amiodarone-loaded PEGylated liposomes (Table 1).

Accumulation of Fluorescence-labeled Nano-sized Beads in the I/R Myocardium

Representative pictures obtained by fluorescence imaging are shown in Fig. 2a (whole heart) and b (sliced hearts). Quantitative analysis revealed that the average fluorescence intensity of the whole heart (Fig. 2c left) or the left ventricle (Fig. 2c right) of the I/R hearts was significantly higher than that in sham-operated hearts.

Amiodarone Concentration in the Blood and I/R Myocardium

The plasma concentration after the administration of liposomal amiodarone was significantly higher than that of free amiodarone (Table 2). Importantly, the amiodarone concentration in the I/R myocardium was detectable after the administration of liposomal, but not free, amiodarone (Table 2).

Hemodynamic Effects of Amiodarone and Liposomal Amiodarone

The baseline heart rates were 411±16, 426±14, 427±12, 409±8 and 414±6 beats/min in the saline, empty liposome, amiodarone (3 mg/kg), amiodarone (10 mg/kg) and liposomal amiodarone (3 mg/kg) groups, respectively. The baseline systolic BP was 113±7, 118±10, 111±5, 90±4 and 104±2 mmHg in the saline, empty liposome, amiodarone (3 mg/kg), amiodarone (10 mg/kg) and liposomal amiodarone (3 mg/kg) groups, respectively. There were no significant differences in the baseline HR or systolic BP among the groups tested. The intravenous administration of amiodarone (3 and 10 mg/kg) or liposomal amiodarone reduced both the HR and systolic BP from the baseline, whereas the saline or empty liposomes did not (Fig. 3). The time-course changes of both the HR and systolic BP were significantly smaller in the liposomal amiodarone group (3 mg/kg) compared with the corresponding dose in the free amiodarone group (3 mg/kg) (Fig. 3). The reductions in HR and systolic BP at 1, but not 3, minutes after liposomal amiodarone administration were significantly smaller compared with those following the corresponding dose of amiodarone.

Antiarrhythmic Effects of Amiodarone and Liposomal Amiodarone

Representative electrocardiograms of the rats that received saline, free amiodarone or liposomal amiodarone are shown in Fig. 4. The intravenous administration of liposomal amiodarone (3 mg/kg), but not amiodarone (3 mg/kg), significantly reduced the duration of VT/VF compared with saline (Table 3). Furthermore, the mortality in the group that received liposomal amiodarone (3 mg/kg), but not the corresponding dose of amiodarone (3 mg/kg), was significantly lower than that in the saline group. In the group of rats that received a high dose of amiodarone (10 mg/kg), the VT/VF duration was 36±12 s, and none of the rats died (Table 3), which was similar to the low dose of liposomal amiodarone group (3 mg/kg).

Discussion

In this study, we revealed that 1) liposomal amiodarone was successfully prepared using a thin-film method, 2) the

Table 1 Characterization of liposomes by dynamic light scatter analysis

	Mean diameter (nm)	Polydispersity index	ζ Potential (mV)
PEGylated liposomes (empty liposomes)	111±14	0.124±0.027	−2.1
PEGylated liposomal amiodarone	113±8	0.128±0.040	−3.7

Results represent 4 independent experiments. The values are expressed as the mean ± SD. *PEG* polyethylene glycol

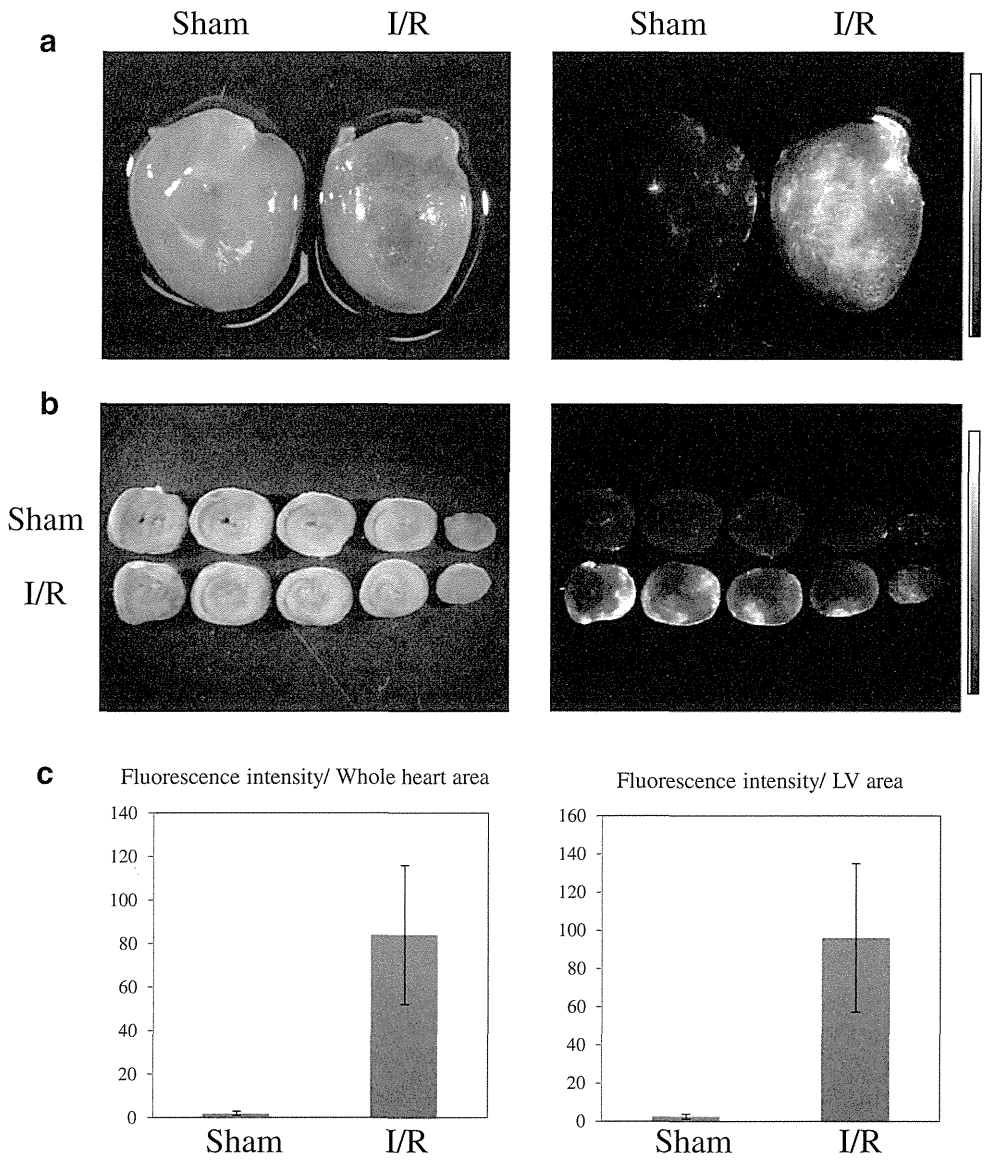

Fig. 2 Representative pictures of ischemia/reperfused myocardium with and without fluorescence-labeled nano-sized beads. Representative pictures obtained by fluorescent imaging are shown in **a** (*whole heart*) and **b** (*sliced hearts*). Quantitative analysis revealed that the average fluorescence intensity of the whole heart (**c** *left*) or the left ventricle (**c** *right*) of the I/R hearts was significantly higher than that of the sham-operated hearts

accumulation of nano-sized beads was observed in the I/R myocardium, 3) liposomal amiodarone showed a smaller reduction in the HR and systolic BP compared with free amiodarone, and 4) liposomal amiodarone, but not amiodarone, reduced the VT/VF duration and mortality during the reperfusion period compared with saline.

Table 2 Amiodarone concentration in the blood and I/R myocardium

Groups	Plasma, ng/mL	Myocardium, ng/mL
Saline	N.D.	N.D.
Free amiodarone	472±147	N.D.
Liposomal amiodarone	3872±378*	71±7*

Data are expressed as the mean ± SEM. *N.D.* not detected. $n=3$ rats in each group. * $p<0.05$ versus free amiodarone

Preparation of Liposomal Amiodarone

This study is the first to encapsulate amiodarone in PEGylated liposomes, although it has been previously encapsulated in other liposomes [22] and micelles [23]. We demonstrated that lipid bilayers composed of unsaturated lipids are more suitable for encapsulating amiodarone in PEGylated liposomes compared with those composed of saturated lipids. PEGylated liposomes have a long circulating time in the bloodstream because PEG endows a steric barrier to liposomes, allowing them to avoid interactions with opsonins and cells of the mononuclear phagocytic system [24]. Thus, they have been used to increase drug stability, safety, and bioavailability in clinical applications. In this study, we found that a higher concentration of amiodarone was retained in the blood when we administered liposomal amiodarone compared with the administration of

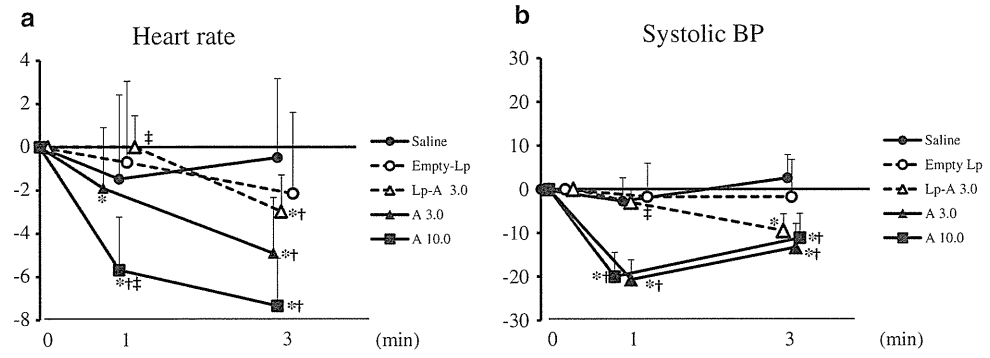

Fig. 3 Time-course changes in HR and systolic BP after drug administration. Shows the percent change from baseline for HR (**a**) and systolic BP (**b**) after intravenous administration of the tested drugs. The data are expressed as the mean ± SEM. *$P<0.05$ versus baseline, paired t-test. $P=0.0009$ (HR), 0.0002 (systolic BP) between amiodarone (3 mg/kg) and liposomal amiodarone (3 mg/kg), 1-way repeated-measurement ANOVA. †$P<0.05$ versus saline, ‡$P<0.05$ versus amiodarone (3 mg/kg), 1-way repeated-measurement ANOVA with Bonferroni's multiple comparison

free amiodarone, suggesting that encapsulation of amiodarone in PEGylated liposomes enhances the stability of amiodarone in the blood.

Targeted Delivery to the I/R Myocardium by Liposomal Amiodarone

Ex vivo fluorescence imaging revealed that fluorescence-labeled nano-sized beads accumulated in the I/R myocardium, suggesting that myocardial permeability can be enhanced in the I/R myocardium. Consistent with this finding, we observed that the amiodarone concentration in the I/R myocardium in the liposomal amiodarone group was much higher compared with that in the amiodarone group. Enhanced permeability in the I/R myocardium and the prolonged presence of amiodarone in PEGylated liposomes in the blood represent a possible mechanism for increased amiodarone concentrations in the I/R myocardium. Amiodarone will be released from accumulated liposomal amiodarone in I/R myocardium due to the natural decay and concentration gradient. These findings suggest that the I/R myocardium is a promising passive target for liposomal drug delivery.

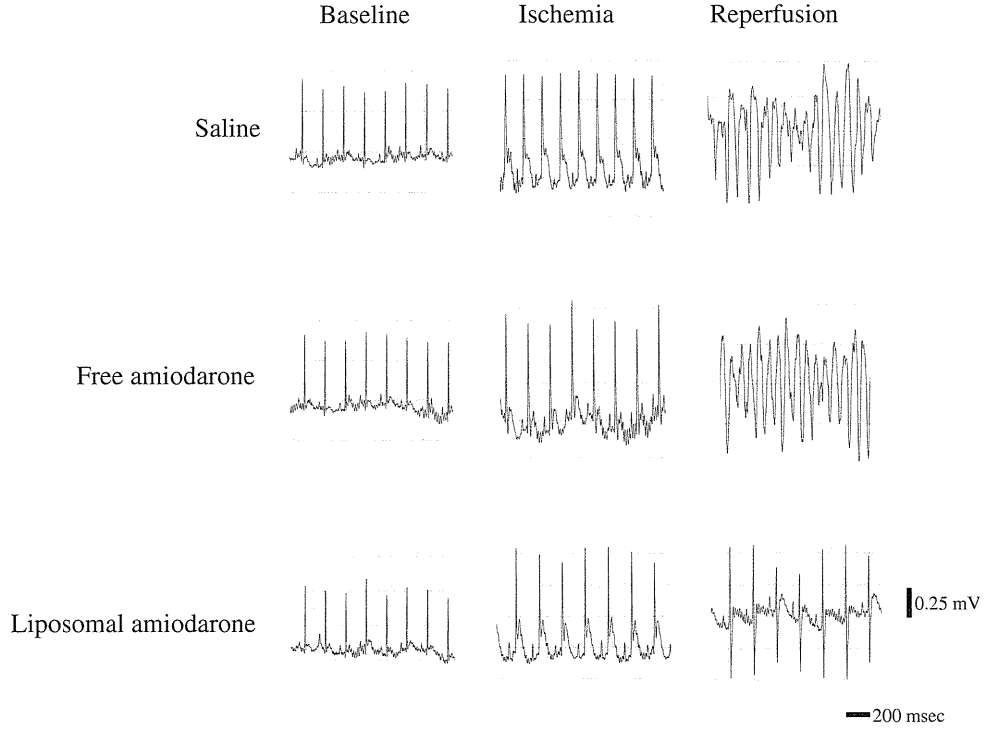

Fig. 4 Representative electrocardiograms. The *upper, middle and lower panels* show representative electrocardiograms under baseline conditions during ischemia and at the onset of reperfusion for rats that received saline, free amiodarone (3 mg/kg) and liposomal amiodarone (3 mg/kg), respectively